JGR Atmospheres

RESEARCH ARTICLE
10.1029/2019JD031093

The Regional Hydroclimate Response to Stratospheric Sulfate Geoengineering and the Role of Stratospheric Heating

I. R. Simpson[1], S. Tilmes[1,2], J. H. Richter[1], B. Kravitz[3,4], D. G. MacMartin[5,6], M. J. Mills[2], J. T. Fasullo[1], and A. G. Pendergrass[1]

[1]Climate and Global Dynamics Laboratory, National Center for Atmospheric Research, Boulder, CO, USA, [2]Atmospheric Chemistry Observations and Modelling Laboratory, National Center for Atmospheric Research, Boulder, CO, USA, [3]Department of Earth and Atmospheric Sciences, Indiana University, Bloomington, IN, USA, [4]Atmospheric Sciences and Global Change Division, Pacific Northwest National Laboratory, Richland, WA, USA, [5]Mechanical and Aerospace Engineering, Cornell University, Ithaca, NY, USA, [6]Department of Computing and Mathematical Sciences, California Institute of Technology, Pasadena, CA, USA

Key Points:
- GLENS geoengineering simulations exhibit substantial precipitation changes, relative to present day
- Stratospheric heating plays a key role in many of the simulated precipitation changes
- Stratospheric heating generally leads to drying in many wet tropical regions

Supporting Information:
- Supporting Information S1

Correspondence to:
I. R. Simpson,
islas@ucar.edu

Citation:
Simpson, I. R., Tilmes, S., Richter, J. H., Kravitz, B., MacMartin, D. G., Mills, M. J., et al. (2019). The regional hydroclimate response to stratospheric sulfate geoengineering and the role of stratospheric heating. *Journal of Geophysical Research: Atmospheres*, *124*. https://doi.org/10.1029/2019JD031093

Received 30 MAY 2019
Accepted 3 NOV 2019
Accepted article online 6 NOV 2019

Abstract Geoengineering methods could potentially offset aspects of greenhouse gas-driven climate change. However, before embarking on any such strategy, a comprehensive understanding of its impacts must be obtained. Here, a 20-member ensemble of simulations with the Community Earth System Model with the Whole Atmosphere Community Climate Model as its atmospheric component is used to investigate the projected hydroclimate changes that occur when greenhouse gas-driven warming, under a high emissions scenario, is offset with stratospheric aerosol geoengineering. Notable features of the late 21st century hydroclimate response, relative to present day, include a reduction in precipitation in the Indian summer monsoon, over much of Africa, Amazonia and southern Chile and a wintertime precipitation reduction over the Mediterranean. Over most of these regions, the soil desiccation that occurs with global warming is, however, largely offset by the geoengineering. A notable exception is India, where soil desiccation and an approximate doubling of the likelihood of monsoon failures occurs. The role of stratospheric heating in the simulated hydroclimate change is determined through additional experiments where the aerosol-induced stratospheric heating is imposed as a temperature tendency, within the same model, under present day conditions. Stratospheric heating is found to play a key role in many aspects of projected hydroclimate change, resulting in a general wet-get-drier, dry-get-wetter pattern in the tropics and extratropical precipitation changes through midlatitude circulation shifts. While a rather extreme geoengineering scenario has been considered, many, but not all, of the precipitation features scale linearly with the offset global warming.

Plain Language Summary This study examines the model-projected hydroclimate changes, relative to present day, that occur when greenhouse gas-driven warming at the end of the 21st century is offset by the injection of sulfate aerosols into the stratosphere. A high greenhouse gas emissions scenario is considered, and the aerosol injection strategy is designed to maintain the global mean temperature, the equator-to-pole temperature gradient, and the interhemispheric temperature gradient. The leading order response in the tropics is a wet-get-drier, dry-get-wetter pattern with substantial drying over India, Amazonia, and parts of Africa. In the midlatitudes, precipitation changes occur in association with shifts of the midlatitude westerlies. Additional experiments are used to assess the role of the dynamical response to warming of the lower stratosphere in producing these responses, and it is found that the dynamical response to warming of the lower stratosphere does, indeed, play an important role in the simulated hydroclimate changes.

1. Introduction

Despite ongoing efforts to reduce anthropogenic carbon emissions, atmospheric greenhouse gas (GHG) levels continue to rise; the planet continues to warm; and the climate continues to change in ways that could have serious impacts on ecosystems and human existence in certain regions of the globe (IPCC, 2013). In light of this, research into so-called "geoengineering" methods that could be used to offset the most

dangerous consequences of human induced climate change is underway (e.g., Keith, 2000). There are, however, many concerns over the adverse effects that geoengineering schemes may have (e.g., Robock, 2008), and it is clear that any consideration of this approach should be informed by a complete understanding of all the potential benefits and adverse consequences it may invoke.

The issue considered here is the potential hydroclimate impacts of stratospheric sulfate aerosol geoengineering, referred to simply as sulfate geoengineering hereafter. This method was proposed in the 1970s as a means to offset a small fraction of GHG-driven warming (Budyko, 1977) and was brought to the forefront of the geoengineering debate by Crutzen (2006). While other aerosols could potentially be used to geoengineer the climate (Blackstock et al., 2009), sulfate has been the most widely studied. This method involves the injection of sulfur bearing gases, most commonly sulfur dioxide (SO_2), into the stratosphere where they are then oxidized to form sulfate aerosols (e.g., Rasch et al., 2008). These aerosols are effective at reflecting and scattering incoming solar radiation and therefore act to cool the surface and the troposphere, but can also absorb infrared radiation (e.g., Stenchikov et al., 1998), resulting in a warming of the lower stratosphere where they reside (e.g., Ammann et al., 2010; Ferraro et al., 2011; Heckendorn et al., 2009; Robock, 2000).

The only observational analog we have of this process is the influence of large volcanic eruptions, such as Mount Pinatubo in 1991. From events like this, we can observe the cooling of the planet induced by the stratospheric aerosols (Robock, 2000) and even some changes in the global hydrological cycle (Iles & Hegerl, 2015; Trenberth & Dai, 2007). However, given the limited number of large volcanic eruptions in the observational record, combined with the highly variable nature of the climate system, determination of regional hydroclimate impacts from the observations alone is extremely challenging, if not impossible. Moreover, historical volcanic eruptions are an imperfect analog to proposed geongineering where the sulfate aerosols are continuously imposed on a much longer timescale, alongside elevated GHG concentrations (Robock et al., 2013). As such, we must also turn to numerical model simulations to identify, and understand, the full impacts of sulfate geoengineering.

Modeling studies have successfully demonstrated the ability of solar radiation management to maintain the globally averaged surface temperature at desired values, whether it be through simple solar dimming or sulfate geongineering (Ammann et al., 2010; Govindasamy & Caldeira, 2000; Kravitz et al., 2013; Muri et al., 2018; Niemeier et al., 2013; Schmidt et al., 2012). While the straightforward implementation of these schemes often results in overcooling of the tropics and undercooling of the poles (Govindasamy & Caldeira, 2000; Kalidindi et al., 2015; Kravitz, Caldeira, et al., 2013), it has been demonstrated that aerosol injections at multiple locations can limit this effect (Kravitz et al., 2016, 2017; MacMartin et al., 2014; Tilmes et al., 2018). However, it is a near certainty that, even if temperature gradients are kept constant, altering the Earth's radiative balances to offset GHG-driven warming will affect the global hydrological cycle. Furthermore, the additional impacts that sulfate geoengineering may have on regional hydroclimate via influences on atmospheric circulation are uncertain and not well understood.

A decline in globally averaged precipitation is a ubiquitous feature of solar radiation management model experiments (Andrews et al., 2009; Bala et al., 2010; Jones et al., 2013; Robock, 2008). The explanation for this decline lies in the effect of increased GHG concentrations without an accompanying increase in globally averaged surface temperature. The response of global mean precipitation to forcings evolves on multiple timescales and can be roughly separated into two components: a part that depends on global mean temperature change (often termed the feedback response) and a part that does not (often termed the rapid adjustment). If sulfate geoengineering eliminates the globally averaged surface temperature change that would otherwise occur under increased GHG concentrations, then the global mean precipitation adjusts according only to the rapid adjustment component of the response. For GHGs, this rapid adjustment is a decline in globally averaged precipitation. This has been argued by Dinh and Fueglistaler (2017) to arise from the weakening of descending motion due to the reduced radiative cooling of the free troposphere. By mass conservation, this weakened descent is accompanied by a synchronous reduction in diabatic ascent and the overall weakening of the circulation results in reduced boundary layer moisture export, and thus reduced precipitation in the global average. In constrast, the rapid adjustment to decreasing solar radiation, for example, as would arise in the presence of increased sulfate aerosols, is expected to be near zero (Andrews et al., 2009; Bala et al., 2010; Samset et al., 2016; Tilmes et al., 2013).

The fact that global precipitation declines under these forcings is expected from consideration of either the atmospheric or surface energy balances (Kravitz et al., 2013). From the atmospheric perspective, increased

GHGs reduce the net longwave cooling of the atmosphere, and this is approximately compensated for by a reduction in diabatic heating associated with the global precipitation decline. In equilibrium, this reduced precipitation must be balanced by reduced evaporation, and the surface energy balance under sulfate geoengineering indicates that this reduced evaporation is primarily compensated for by reduced incoming solar radiation (Bala et al., 2008). In the case of sulfate geoengineering, the precipitation decline can be further enhanced by the greenhouse effect of the sulfate aerosols themselves (Niemeier et al., 2013), although this appears to be model- or method-dependent (Xia et al., 2017).

There are a number of additional reasons why regional circulation and hydroclimate might be expected to change with geoengineering. For one thing, while in the global average, the surface temperature changes are limited by the geoengineering; this need not be the case locally, and so, for example, altered land-sea temperature contrasts or altered latitudinal gradients in temperature could impact on the circulation and precipitation. In addition, as discussed by Bony et al. (2013), the presence of enhanced GHG concentrations in the atmosphere would still be expected to weaken the tropical circulation even in the absence of surface warming, for instance in a geoengineering scenario, since the reduced net longwave cooling of the atmosphere under elevated GHGs will affect the strength of atmospheric vertical motions, leading to regional patterns of precipitation change. Then, specific to the case of sulfate geoengineering, the lower stratosphere warms due to the aborption of radiation by the sulfate aerosols, and this warming could then induce dynamical responses. These could arise as altered stratospheric temperatures drive shifts in the midlatitude westerlies and storm tracks (Ferraro et al., 2013; Richter et al., 2018) or impact on the tropical circulation (Ferraro et al., 2014).

A number of studies have considered the effects of solar dimming on regional hydroclimate in multiple models within the Geoengineering Model Intercomparison Project framwork (Kravitz et al., 2013). Tilmes et al. (2013) note the substantial reduction of precipitation over land areas in many of the monsoon regions, and Smyth et al. (2017) further relate this to altered interhemispheric temperature gradients and changes to the seasonal migration of the intertropical convergence zone. Jones et al. (2013) point out that the overall impact of solar dimming on global mean precipitation is dependent on the fraction of global warming that is being compensated, and Irvine et al. (2019) recently demonstrated that using solar dimming to only halve the amount of global warming, successfully moderates the hydroclimate impacts of rising GHGs over the majority of land regions. However, given the possible role that stratospheric heating may play in the case of sulfate geoengineering, the extent to which these solar dimming results are of relevance to the sulfate geoengineering response is unclear. Robock et al. (2008), Rasch et al. (2008), and Jones et al. (2010) each considered the impact of sulfate geoengineering, as opposed to solar dimming, and while Robock et al. (2008) also found a weakening of the Asian and African monsoons, Rasch et al. (2008) find differences in their pattern of precipitation change using a different model. Using an intermediate complexity model, Ferraro et al. (2014) demonstrate a weakening of the tropical circulation and accompanying precipitation changes and argue for the important role played by the stratospheric heating in this response.

The goals of the present study are twofold. The first is to present a detailed description of regional hydroclimate change within a large ensemble of fully coupled stratospheric sulfate geoengineering simulations. These simulations have been performed with the Community Earth System Model Version 1 (CESM1) with the Whole Atmosphere Community Climate Model (WACCM) as its atmospheric component (CESM1[WACCM]). WACCM has a well-resolved stratosphere, and the geoengineering is simulated through SO_2 injections with the resulting aerosol concentrations determined prognostically by the model. Furthermore, the geoengineering has been designed to maintain not only globally averaged surface temperature but also the equator-to-pole and interhemispheric temperature gradients. These simulations are, therefore, a step up in complexity compared to those that have been considered before. In addition, with a larger ensemble of simulations than typically used in geoengineering studies (20 members), the hydroclimate changes can accurately be placed within the context of internal climate variability. The second goal is to assess the potential role that stratospheric heating may play in producing this hydroclimate change and this is achieved through idealized stratospheric heating experiments with CESM1 (WACCM). The model simulations and analysis methods are described in section 2. We then give a brief overview of changes in the global radiative balance and large scale circulation in the model experiments in section 3 before providing an analysis of regional hydroclimate change in section 4. Discussion is provided in section 5 before conclusions are drawn in section 6.

Table 1
Summary of Community Earth System Model Version 1 (Whole Atmosphere Community Climate Model) Experiments

Name	Number of Members × Length	Description
BASE	20 × 21 years	Simulations from 2010–2030 run under RCP8.5 forcings
RCP8.5	3 × 21 years	Years 2075–2095 of a three-member ensemble run from 2010 to 2099 under RCP8.5 forcings
GLENS	20 × 21 years	Years 2075–2095 of 20 simulations run from 2020 to 2099 under RCP8.5 forcing with sulfate geoengineering using "feedback-control"
GEOHEAT	4 × 21 years	Simulations from 2010 to 2030 under RCP8.5 forcings with additional temperature tendencies imposed in the stratosphere derived from GLENS
GEOHEAT_S	80×14 months	As GEOHEAT but initialized from 1 January for each year of four BASE members and run for 14 months with stratospheric heating imposed

Note. GLENS = Geoengineering Large Ensemble, RCP8.5 = Representative Concentration Pathway 8.5.

2. Model Experiments and Methods

2.1. Model Experiments

2.1.1. Sulfate Geoengineering and Accompanying RCP8.5 Experiments

We make use of an ensemble of CESM1(WACCM) simulations that have been made available through the Geoengineering Large Ensemble (GLENS) project and are described in detail in Tilmes et al. (2018). In brief, these make use of CESM1.5 (Hurrell et al., 2013) and the version of WACCM that was introduced by Mills et al. (2017). It has a latitude×longitude resolution of $0.9^o \times 1.25^o$ and 70 layers in the vertical extending to 140 km. WACCM has fully interactive middle atmosphere chemistry (Mills et al., 2017) and is coupled to the Parallel Ocean Program Version 2 ocean model and the Community Land Model Version 4.5 (CLM4.5). Of relevance for the simulation of geoengineering, CESM1(WACCM) simulates the formation of sulfate aerosols from SO_2 injections through oxidation, using the Modal Aerosol Module (Liu et al., 2012). In addition, through its parameterization of leaf stomatal conductance and photosynthesis, CLM4.5 allows plant physiology to respond to rising CO_2 levels and altered direct and diffuse radiation. However, monthly vegetation distributions are prescribed and do not evolve in response to forcings. CESM1(WACCM) compares well with observations in many respects (Mills et al., 2017), and a comparison of its precipitation climatology with observations over land is given in supporting information, Figure S1.

Table 1 provides a summary of the simulations and the periods of analysis that will be used in this study. Our control simulations (BASE), representative of present day climate, are a 20 member ensemble, with each member initialized in 2010 and set to follow the Representative Concentration Pathway 8.5 (RCP8.5) scenario (Taylor et al., 2012) to 2030. These 20 simulations are each initialized from the same, previously spun-up, state and differ in the addition of a round-off level noise perturbation to the air temperature field. Three of these RCP8.5 members were extended out to 2097, and the average over the period 2075 to 2095 of these simulations will be referred to as "RCP8.5".

From the year 2020, of each of the BASE members, an ensemble of 20 sulfate geoengineering experiments was initialized, and these will be referred to as "GLENS." These evolve under RCP8.5 forcing until 2097 but with additional SO_2 injections at four locations in the stratosphere (15^oN and 15^oS at 25 km and 30^oN and 30^oS at 22.8 km and an arbitrary longitude of 180^oE). The injection amounts and locations are chosen each year based on the feedback-control algorithm described in Kravitz et al. (2016, 2017) and MacMartin et al. (2014) and are aimed at maintaining three temperature targets at the climatological average of 2015 to 2025 of the first 13 BASE members: the globally averaged surface temperature; the interhemispheric temperature gradient; and the equator-to-pole temperature gradient. The first two temperature targets are maintained very well, and only minor deviations of the third occur by the end of the century (see Tilmes et al. (2018), their figure 1). Our primary focus in these GLENS experiments will be the period from 2075 to 2095.

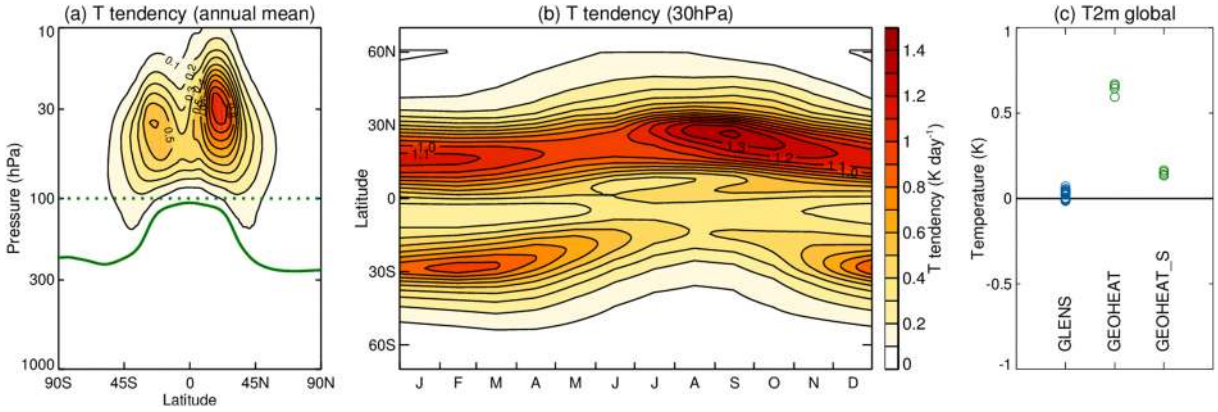

Figure 1. (a) Zonal mean annual mean temperature tendency (Q_{SO_4}) derived according to equation (1). In GEOHEAT, these temperature tendencies are imposed only above the 100-hPa level (green dotted line). In GEOHEAT_S, these temperature tendencies are imposed only above the monthly climatological lapse rate tropopause of 2075–2095 in GLENS, and the annual mean of this is shown by the green solid line. (b) The seasonal cycle of zonal mean Q_{SO_4} at the 30-hPa level (only 70°S to 70°N is shown). (c) The globally averaged near surface (2 m) air temperature anomalies compared to BASE for the 20 GLENS members (left, blue), the 4 GEOHEAT members (middle, green), and the mean of the 20 GEOHEAT_S members initialized from the four different BASE members (right, green). GLENS = Geoengineering Large Ensemble.

2.1.2. Stratospheric Heating Experiments

We perform two additional sets of stratospheric heating experiments with the same model version as GLENS. In these, a zonally symmetric, seasonally varying temperature tendency (Q_{SO_4}) is added to the prognostic equation for temperature to mimic the additional heating caused by the sulfate aerosols in GLENS. Q_{SO_4} is derived from a double call to the radiation scheme that was performed in both BASE and GLENS. In the first call, the radiation scheme is called as normal and is allowed to see all constituents within the atmosphere, resulting in the atmospheric heating rate Q_1. In the second call, performed purely for diagnostic purposes, the radiation scheme sees all atmospheric constituents, except aerosols, yielding the heating rate Q_2. The difference in the temperature tendency between GLENS and BASE that arises due to the excess sulfate aerosol can be approximated as

$$Q_{SO_4}(\phi, p, m) = [Q_1 - Q_2]_{\mathrm{GLENS}}(\phi, p, m) - [Q_1 - Q_2]_{\mathrm{BASE}}(\phi, p, m), \quad (1)$$

where ϕ, p and m refer to latitude, model level, and month of the year, $[.]_{\mathrm{GLENS}}$ refers to the zonally averaged seasonally varying climatology over 2075–2095 of all GLENS members, and $[.]_{\mathrm{BASE}}$ refers to the same over 2010–2030 of all BASE members. $[Q_1 - Q_2]_{\mathrm{BASE}}$ is small but non-zero due to the influence of other aerosol species in the BASE climate and equation (1) is an approximation for the heating rate due to sulfate aerosols because there may be changes in other aerosol constituents between GLENS and BASE included in Q_{SO_4}. Ultimately, however, Q_{SO_4} is dominated by the heating rates arising from the increased stratospheric sulfate aerosol. The zonal mean annual mean Q_{SO_4} is shown in Figure 1a, and its seasonal cycle at 30 hPa is shown in Figure 1b. Heating rates are larger in the Northern Hemisphere because the feedback control algorithm determines that a greater proportion of SO_2 injections is needed there to maintain the three temperature targets (see Tilmes et al. (2018), their figures 2 and 4). In practice, Q_{SO_4} is updated every 6 hr in the model to the linear interpolation between monthly averages centered at the middle of each month of the year.

In the first stratospheric heating experiment, "GEOHEAT", the simulations are performed exactly as BASE, that is, initialized from 2010 and run until 2030 under RCP8.5 forcings, but they differ in that the additional heating, Q_{SO_4}, is imposed above 100 hPa (green dotted in Figure 1a). Four members were performed, yielding 84 years of simulation. The addition of Q_{SO_4} in GEOHEAT successfully results in a change in temperature in the lower stratosphere that is similar to that of GLENS, that is, a warming of around 10K centered on the equator around 70 hPa (compare Figure 2c with 2b). What is absent in GEOHEAT is the additional stratospheric cooling due to the increased GHG concentrations.

A complicating factor in GEOHEAT is a global warming that likely arises as a result of increased stratospheric water vapor. In GLENS, the stratospheric water vapor concentration is almost double that of BASE (Figures 2f and 2e) which is expected given the warming of the tropical lower stratosphere and the cold-point tropopause (Richter et al., 2018). Indeed, in the GEOHEAT experiments, stratospheric water vapor also

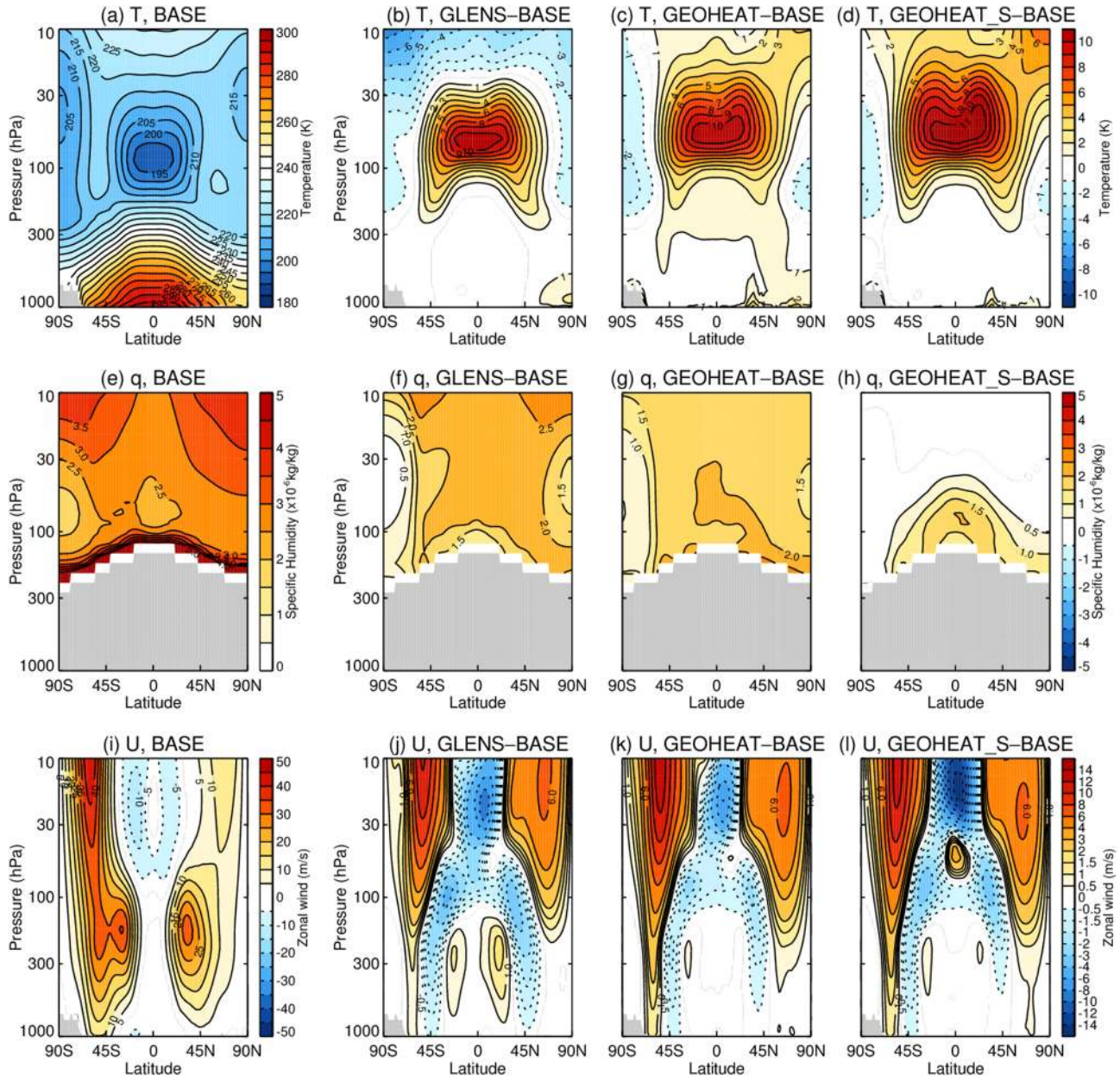

Figure 2. (a)–(d) Annual mean, zonal mean temperature, (K) for BASE, GLENS−BASE, GEOHEAT−BASE, and GEOHEAT_S−BASE, respectively. (e)–(h) As (a)-(d) but for zonal mean specific humidity (kg/kg). Tropospheric specific humidity has not been plotted for clarity. (i)–(l) As (a)–(d) but for zonal mean zonal wind. Note the nonlinear contour interval for (j)–(l). GLENS = Geoengineering Large Ensemble.

increases (Figure 2g), although not by quite as much as in GLENS, probably because the stratosphere has seen warmer cold point temperatures for a shorter time. Through its greenhouse effect, increased stratospheric water vapor would be expected to warm the troposphere and surface (Forster & Shine, 1999, 2002; Manabe & Wetherald, 1967) and cool the stratosphere (Maycock et al., 2011). In GLENS, the SO_2 injections are continually tuned to maintain the surface temperature targets and, therefore, compensate for the additional surface warming due to stratospheric water vapor (Figure 1c left). In GEOHEAT, however, there is no such compensation, and the surface warms by ~ 0.6°C (Figure 1c middle).

To ensure that conclusions drawn from GEOHEAT as to the role of stratospheric heating are not critically dependent on the globally averaged warming, which is an artifact of the experimental design, we also consider a spin-up ensemble, or GEOHEAT_S. Each member of GEOHEAT_S is initialized from 1 January of individual years of BASE. In total, we use four members of BASE, that is, 80 initialization dates (years

2011–2030 for each member). Each GEOHEAT_S simulation is run for 14 months with the same Q_{SO_4} perturbation imposed as in GEOHEAT. Although, instead of imposing Q_{SO_4} above 100 hPa, we impose it above the monthly climatological lapse rate tropopause (Reichler et al., 2004) of GLENS (green solid in Figure 1a) to also test the sensitivity to inclusion of the subtropical lobes of stratospheric heating.

The stratospheric temperature anomalies in GEOHEAT_S reach comparable values to GLENS after 2 months, as can be seen from the annual mean temperature anomalies in Figure 2d, where the annual mean has been taken from 1 March of the first year of GEOHEAT_S to the end of February of the second year. Since these simulations are only 14-months long, stratospheric water vapor has not had the chance to fully evolve (Figure 2h) and, while there is a slight global average warming, it is much reduced compared to GEOHEAT (Figure 1c, right). When the annual mean for GEOHEAT_S is shown, it is the average from the beginning of March of year 1 to the end of February of year 2, and for the June-July-August (JJA) and December-January-February (DJF) seasons, we show the average of the 6th to 8th months and the 12th to 14th months, respectively.

The GEOHEAT_S experiments have the advantage over GEOHEAT that the influence of the globally averaged warming in the presence of increased stratospheric water vapor has been minimized. However, they are designed such that any aspect of the response to stratospheric heating that depends on changes in the ocean circulation that evolve on longer timescales will not have a chance to be realized. Nevertheless, aspects of the response that are common to both GEOHEAT and GEOHEAT_S can be considered to not depend critically on (a) the global averaged warming that is present in GEOHEAT, (b) the details of the lower boundary above which Q_{SO_4} is imposed or (c) the evolution of the ocean on timescales longer than is allowed within GEOHEAT_S.

To summarize, the difference between GLENS and BASE will be used to identify the impact of the sulfate geoengineering, and this will be compared with the impacts of GHG-driven warming determined via RCP8.5−BASE. The GLENS−BASE difference will be further compared with GEOHEAT−BASE and GEOHEAT_S−BASE to identify the aspects of the geoengineering response in which the stratospheric heating plays a key role. Ultimately, the hydroclimate response produced in these simulations will be a result of both the direct influence of the forcing agents and the ensuing feedbacks that evolve as the climate system responds (Myhre et al., 2017). In the case of GLENS, the direct forcings that we expect could drive hydrological cycle changes are the reduction in radiative cooling of the atmosphere in the presence of enhanced GHG concentrations (Bony et al., 2013), the radiative effects at the surface that result from the enhanced GHG concentrations and enhanced sulfate aerosol concentrations and their imperfect compensation for one another, the dynamical and radiative influences of warmer temperatures in the lower stratosphere (Ferraro et al., 2014), and altered evapotranspiration resulting from changes in plant physiology under both elevated CO_2 levels and changes in the ratio of direct to diffuse radiation (Fyfe et al., 2013; Xia et al., 2017). In contrast, in GEOHEAT and GEOHEAT_S, only the dynamical and radiative influences of warmer temperatures in the lower stratosphere will be present.

2.1.3. CMIP5 Simulations

When considering precipitation changes over land in section 4, we also present the Coupled Model Intercomparison Project, phase 5 (CMIP5) multimodel mean precipitation change between 2075–2095 and 2010–2030 under RCP8.5 for comparison with the CESM1(WACCM) RCP8.5−BASE difference. This is so the extent to which the climate change response in CESM1(WACCM) is representative of other model projections can be assessed. In total, 36 models are used, as summarized in supporting information, Table S1. For models with multiple members, the ensemble mean is first calculated.

2.2. Analysis Methods

Our focus is on regional hydroclimate change and for the majority of regions this will be presented for both the summer and winter seasons. For precipitation changes in the annual mean and other seasons, see supporting information, Figure S2. The primary comparison between GLENS, RCP8.5, and the stratospheric heating experiments is made through precipitation (P), since the major factors that contribute to evaporation changes in GLENS will not be present with stratospheric heating alone as the surface energy balance and plant physiology will not be altered in the same way. However, global overviews of evaporation (E) and precipitation − evaporation ($P - E$) are also provided along with regional comparisons of these fields and soil moisture integrated over the top 5 CLM4.5 levels (roughly 29 cm) for particular locations. The majority of locations chosen for this comparison are those where precipitation declines in GLENS.

For completeness, we cover much of the global land surface in our analysis, but our discussion will primarily focus on three regions where stratospheric heating is found to play an important role: the Asian summer monsoon (section 4.3); South America (section 4.4); Europe and the Mediterranean (section 4.5). We only briefly summarize the key points for Australia, Africa, and North America in section 4.6. Where averages are performed over specific countries or states, this has been achieved using the shapefiles provided at https://gadm.org/download_country_v3.html. There are many other aspects of hydroclimate that could have important societal implications, such as extreme precipitation or drought occurrence, and we do not consider these here. Rather, our focus is primarily on mean precipitation changes and the extent to which these result from a dynamical response to heating of the lower stratosphere. A more detailed global investigation of soil moisture changes in these experiments is provided by Cheng et al. (2019).

The significance of the difference between GLENS and BASE is determined using a Student's t-test on the difference between the two 20 member ensemble means, treating each member as an independent sample. For the significance of anomalies in RCP8.5, GEOHEAT, and GEOHEAT_S, since they have fewer members, we use a bootstrapping with replacement methodology whereby an equivalent number of members to that in the experiment (3 for RCP8.5 and 4 for GEOHEAT and GEOHEAT_S) is resampled, with replacement, from BASE and the mean taken. This is repeated 1,000 times, and where the experiment mean lies outside of the 5th to 95th percentile range of these BASE subsamples, it is considered significant. This is equivalent to a one-sided test at the 95% level.

When comparing regional precipitation changes over land between GLENS and GEOHEAT or GEOHEAT_S, the spatial pattern correlation (r) is quoted along with a p value (p). The p value is the probability of obtaining this magnitude of r from random sampling of internal variability, accounting for spatial autocorrelation in the field. This is determined by bootstrapping, with replacement, an equivalent number of members of BASE to that in GEOHEAT or GEOHEAT_S and taking the difference from the BASE ensemble mean. The pattern correlation between this subsample and the GLENS−BASE ensemble mean difference is calculated. This is repeated 1,000 times, and the p value reflects the percentile of the distribution of obtained correlations that is closest to the pattern correlation determined from the experiment, r.

The uncertainty range on the ensemble mean P, E, $P-E$, and surface energy budget contributions is determined using bootstrapping with replacement on the individual years that make up the ensemble mean, assuming each year is independent. One thousand bootstrapped differences between each experiment and BASE are determined, and the confidence interval given on the ensemble mean is the 5th to 95th percentile range of these differences.

For the CMIP5 models, regions where more than two-thirds of the models agree on the sign of the change are considered to have high model agreement.

3. Overview of the Global Surface Energy Balance and Large Scale Circulation Response

3.1. Global Surface Energy Balance

As described in the introduction, a reduction in globally averaged precipitation is expected when increased GHG concentrations are compensated for by reduced insolation. By 2075–2095, the geoengineering in GLENS is offsetting the surface warming of almost 4 K that occurs in RCP8.5. This is accompanied by a globally averaged decline in precipitation of ~3% (Figure 3a). The surface energy balance indicates, as expected, that geoengineering reduces the net downwelling shortwave, and the dominant term that offsets this is the reduced evaporation, with a secondary role for anomalous net upward longwave (LW; Figure 3a). The reduction in evaporation is equal to the reduced precipitation. A net residual remains in the balance because of the net energy transfer to the ocean which is larger in BASE than in GLENS (Fasullo et al., 2018).

In GEOHEAT and GEOHEAT_S (Figures 3b and 3c), the changes in globally averaged net radiative fluxes and precipitation are much smaller, as expected. In GEOHEAT, the net downwelling surface longwave shows a small increase and is accompanied by a small increase in evaporation and precipitation. This is likely due to the radiative forcing from the increased stratospheric water vapor and ensuing tropospheric feedbacks as the planet warms slightly (Forster & Shine, 1999, 2002; Manabe & Wetherald, 1967). In GEOHEAT_S, changes in the radiative fluxes are small, but there is a net downward energy flux associated with a globally averaged reduction in evaporation (accompanied by reduced precipitation) as the system responds to the imposed stratospheric heating.

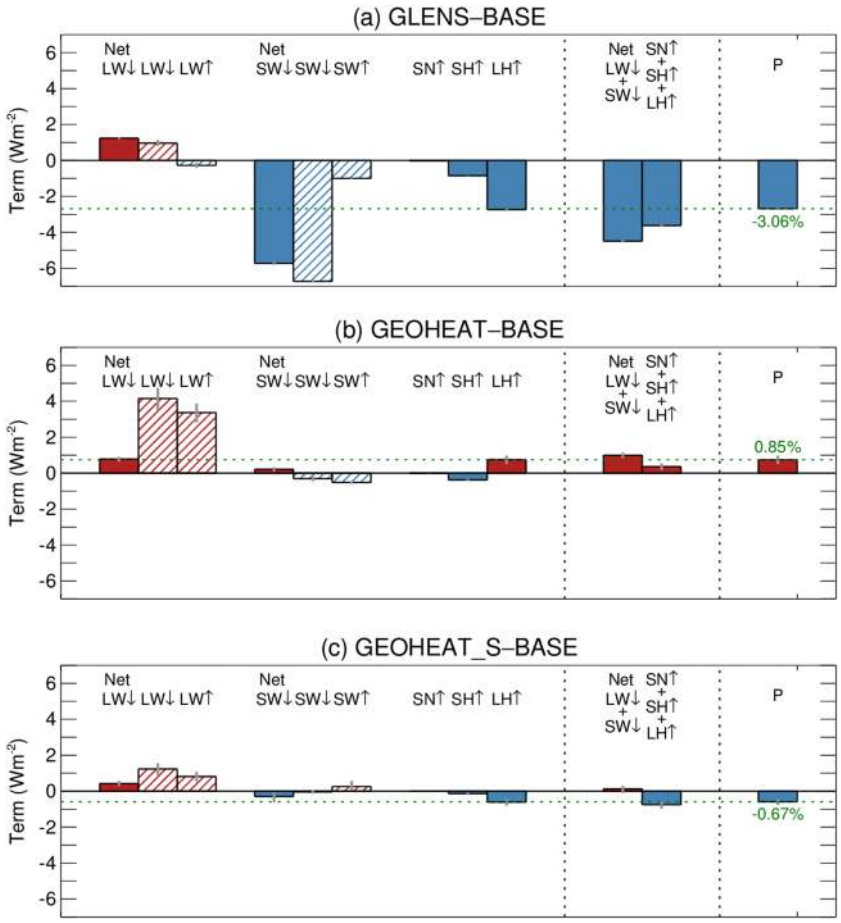

Figure 3. Globally averaged surface energy balance for (a) GLENS−BASE, (b) GEOHEAT−BASE, and (c) GEOHEAT_S−BASE. In each panel, the left section shows, from left to right, net downward longwave radiation (LW↓) with the subsequent hatched bars depicting the downward and upward contributions to the net; net downward shortwave radiation (SW↓) with the subsequent hatched bars depicting the downward and upward contributions to the net; upward heat flux associated with snow melting as it lands on the ocean surface (SN↑); upward sensible heat flux (SH↑); and upward latent heat flux (LH↑). The middle section then shows (left) the sum of the net downward radiative fluxes and (right) the sum of the upward turbulent fluxes and the snow melting contribution. The right section and green dotted line show the precipitation change expressed in Wm^{-2}, that is, precipitation in m/s scaled by ρL_v, where ρ is the density of liquid water at standard temperature and pressure (1,000 kg/m^3) and L_v is the specific latent heat of vaporization at 0°C (2.5×10^6 J/kg). The percent change in globally averaged precipitation is also quoted in green. Gray vertical lines on each bar depict the 5th to 95th percentile range determined via bootstrapping as described in section 2.2. GLENS = Geoengineering Large Ensemble.

The important point to take from Figure 3 for the following analysis is that, in the stratospheric heating experiments, we have not perturbed the energy balances in the same way as in GLENS. Mechanisms associated with the reduced incoming shortwave radiation or the enhanced atmospheric GHG concentrations will not be present. All that is present is the dynamical response to the warming of the lower stratosphere.

3.2. Large Scale Circulation

In GLENS, stratospheric westerly anomalies occur in the extratropics in the annual mean (Figure 2j) due to the heating of the tropical lower stratosphere (Figures 2k and 2l). The tropospheric zonal wind responses in the JJA and DJF seasons can be examined more thoroughly by consideration of the 850-hPa zonal wind anomalies (U850) in Figures 4 and 5 (top). The 850-hPa level is representative of the eddy-driven midlatitude westerly jet stream, and given the equivalent barotropic nature of the extratropical circulation, results are similar throughout the depth of the lower troposphere (not shown). Only the response in GEOHEAT is shown here but GEOHEAT_S is shown in supporting information, Figure S3, and the difference between the GLENS and GEOHEAT responses and their significance are shown in supporting information, Figure S4. In GLENS, the zonal wind anomalies are in the sense to shift the Southern Hemisphere (SH) westerlies

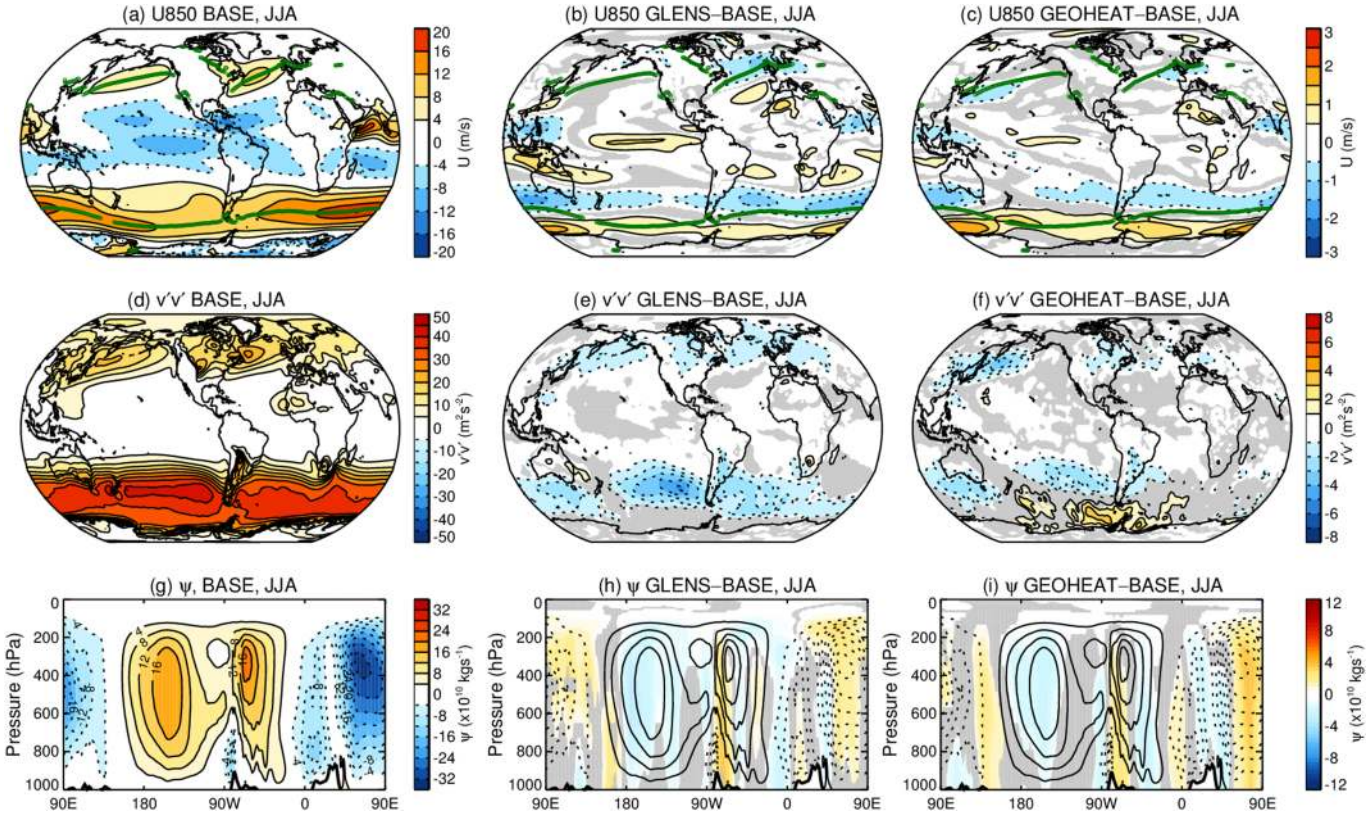

Figure 4. JJA circulation. (top) A 850-hPa zonal wind, (middle) 850 hPa 10-day high pass meridional wind variance ($v'v'$), and (bottom) zonal stream function averaged over 5°S to 5°N. (Left) BASE climatology, (middle) GLENS−BASE difference, and (right) GEOHEAT−BASE difference. The green markings at each longitude in (a)–(c), which merge over the ocean basins into a line, show the latitude of the BASE jet maximum at each longitude and the black line in (g)–(i) shows the climatological surface pressure averaged over 5°S to 5°N. Gray regions in the difference plots are where the difference is not significantly different from zero at the 95% level by the methods outlined in section 2.2. GLENS = Geoengineering Large Ensemble, JJA = June-July-August.

poleward in both DJF and JJA. These zonal wind anomalies are actually of comparable magnitude to those that occur by 2075–2095 under continued global warming (not shown, but see figure 4 of Simpson et al., 2014, for CMIP5 models). The zonal wind anomalies in GLENS are almost entirely reproduced in GEOHEAT (compare panels b and c in Figures 4 and 5). In fact, the response in DJF is actually larger in GEOHEAT. This indicates that the stratospheric heating plays a dominant role.

In the Northern Hemisphere, the wind response is more complex. In JJA, the anomalies are weak, and while GLENS exhibits a slight equatorward shift of the westerlies, the response in GEOHEAT is primarily a weakening (Figures 4b and 4c). In DJF, there is a poleward shift of the North Atlantic westerlies in GLENS (Figure 5b), and this is reproduced rather well in GEOHEAT (Figure 5c) with some minor, albeit significant, differences in the magnitude and location of the anomalies (see Figure S4d for the difference plot). In contrast, in the Pacific, the GLENS and GEOHEAT responses are very different. In GLENS, there is an equatorward shifting of the midlatitude westerlies (Figure 5b), while in GEOHEAT, there is a weakening (Figure 5c) so stratospheric heating is not the dominant contributor to the extratropical circulation change in the North Pacific.

The accompanying changes in storm track activity as represented by the 10-day high pass filtered (Lanczos filtered with 181 weights) meridional wind variance ($v'v'$) at 850 hPa reveal substantial differences between GLENS and GEOHEAT (compare panels e and f of Figures 4 and 5, or alternatively see Figures S4b and S4e for the difference plot with significance). In the absence of other effects, storm track activity would be expected to mirror changes in U850 since U850 is related to both baroclinicity and the steering of the storm systems. In GEOHEAT this is broadly the case (Figures 4 and 5f), but in GLENS, the storm track activity is weakened everywhere (Figures 4 and 5e) and to a greater extent than in GEOHEAT. In GLENS, something

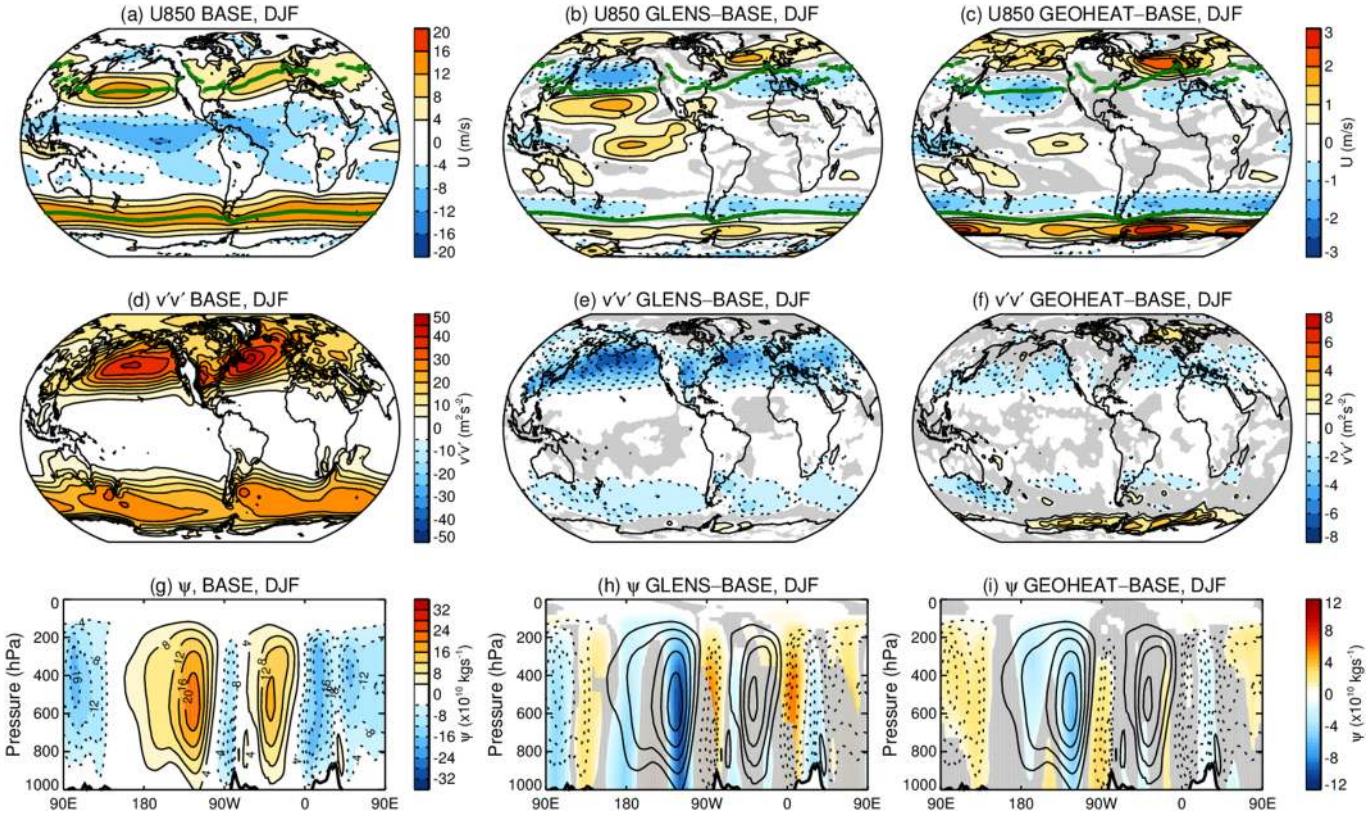

Figure 5. DJF circulation. (top) A 850-hPa zonal wind, (middle) 850 hPa 10-day high pass meridional wind variance ($v'v'$), and (bottom) zonal stream function averaged over 5°S to 5°N. (Left) BASE climatology, (middle) GLENS−BASE difference, and (right) GEOHEAT−BASE difference. The green markings at each longitude in (a)–(c), which merge over the ocean basins into a line, show the latitude of the BASE jet maximum at each longitude and the black line in (g)–(i) shows the climatological surface pressure averaged over 5°S to 5°N. Gray regions in the difference plots are where the difference is not significantly different from zero at the 95% level by the methods outlined in section 2.2. DJF = December-January-February, GLENS = Geoengineering Large Ensemble.

related to the combined influence of geoengineering and rising GHGs is acting to weaken the storm track activity, and this is not accounted for by the stratospheric heating influence alone.

An overview of changes in the tropical divergent circulation is provided by the zonal stream function (Ψ) anomalies in Figures 4 and 5g–i, calculated from the divergent component of the zonal wind averaged from 5°S to 5°N following Yu and Zwiers (2010). In JJA, the Ψ anomalies in GLENS and GEOHEAT are very similar (compare Figures 4h and 4i). Both exhibit a weakening of the Pacific Walker Circulation between the dateline and 90°W and the Indian Ocean overturning circulation to the west. In GEOHEAT_S, the divergent circulation in the tropical Pacific has not evolved, presumably since the Sea Surface Temperatures (SSTs) have not yet fully responded (see below and Figure S3d). In DJF, the response is more complex. Again, in GEOHEAT, the response is predominantly a weakening of the climatological circulation (Figure 5i), but in GLENS, the weakening of the Pacific Walker Circulation is greater than in GEOHEAT, and there is more structure in the anomalies to the west. Therefore, the influence of stratospheric heating is to weaken the zonal overturning circulation in the tropics, in line with the results of Ferraro et al. (2014). In JJA, this appears to explain almost the full GLENS response, but in DJF, other factors seem to play an important role.

It is challenging to unambiguously identify causal mechanistic pathways through diagnosis of quasi equilibrium experiments like these, as the whole system has attained a new balance with roles for both the ultimate drivers and ensuing feedbacks in the responses found. However, for the poleward shifting of the westerlies, we can draw from previous literature. A poleward shifting of the midlatitude westerlies is a typical response to stratospheric heating and/or strengthening of the polar vortex in idealized modeling studies (DallaSanta et al., 2019; Haigh et al., 2005; Polvani & Kushner, 2002; Simpson et al., 2009), and a localized poleward shift in the North Atlantic westerlies occurs when the stratospheric vortex is anomalously strong

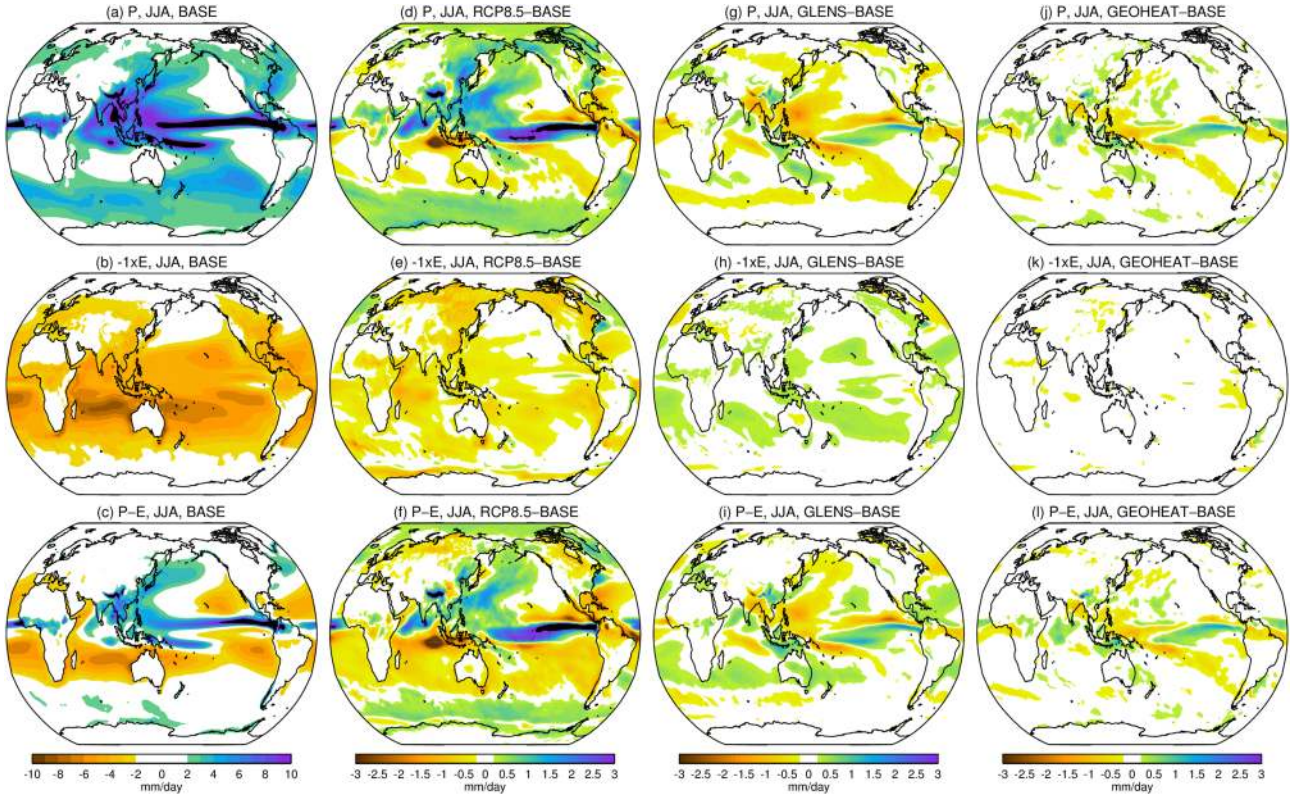

Figure 6. (a)–(c) JJA averaged precipitation, −1× evaporation and precipitation−evaporation for BASE. (d)–(f)/(g)–(i)/(j)–(l) are as (a)–(c) but for RCP8.5−BASE, GLENS−BASE, and GEOHEAT−BASE. GLENS = Geoengineering Large Ensemble, JJA = June-July-August.

in observed, interannual variability (Baldwin & Dunkerton, 2001). Mechanisms have been proposed, involving the response of transient eddies (e.g., Simpson et al., 2009; Wittman et al., 2007) or planetary scale waves (e.g., Song & Robinson, 2004) to the stratospheric forcing in these contexts.

For the aspects of the response that differ in GLENS, from those in GEOHEAT, such as the overall weakening of the transient eddy activity, the equatorward shift of the westerlies in the Pacific, the smaller magnitude of the poleward shift of the westerlies in the SH during DJF, and the difference in tropical divergent circulation during DJF, a reasonable speculation is that this is related to the elevated atmospheric GHG concentrations and/or the reduced evaporation. These will alter the magnitude and distribution of diabatic heating associated with precipitation, and the increased GHGs will alter the atmospheric LW cooling. For the storm track differences, the reduction in LW cooling under elevated GHG levels may be expected to lead to increased stability and reduced precipitation within individual extratropical cyclones which, in turn, may weaken their overall intensity, leading to the reduction in $(v'v')$ found. The weaker poleward shift of the westerlies in the SH and the equatorward shift of the Pacific westerlies during DJF may result from the overall weakening of the storm track activity, which would be expected to lead to a reduced poleward momentum flux. Alternatively, it might be more directly related to the altered distribution of diabatic heating as a result of reduced evaporation and associated differences in moisture transport. There may also be a role for altered latitudinal gradients in temperature that arise due to the radiative effects of the sulfate aerosols. While the equator-to-pole temperature gradient is maintained by the feedback control algorithm for the annual average, this is not necessarily the case seasonally. For the tropics, the GHG-induced reduction in LW cooling and associated weakening of the circulation (Bony et al., 2013) will not be present in the stratospheric heating experiments. In addition, the imperfect compensation, regionally, between the GHG and sulfate influence in GLENS could, for example, lead to a cooling of the land surface relative to the ocean in the summer months, with resulting changes to the circulation (Richardson et al., 2016). However, additional targeted experiments and analysis are needed to assess the contributions of each of these mechanisms.

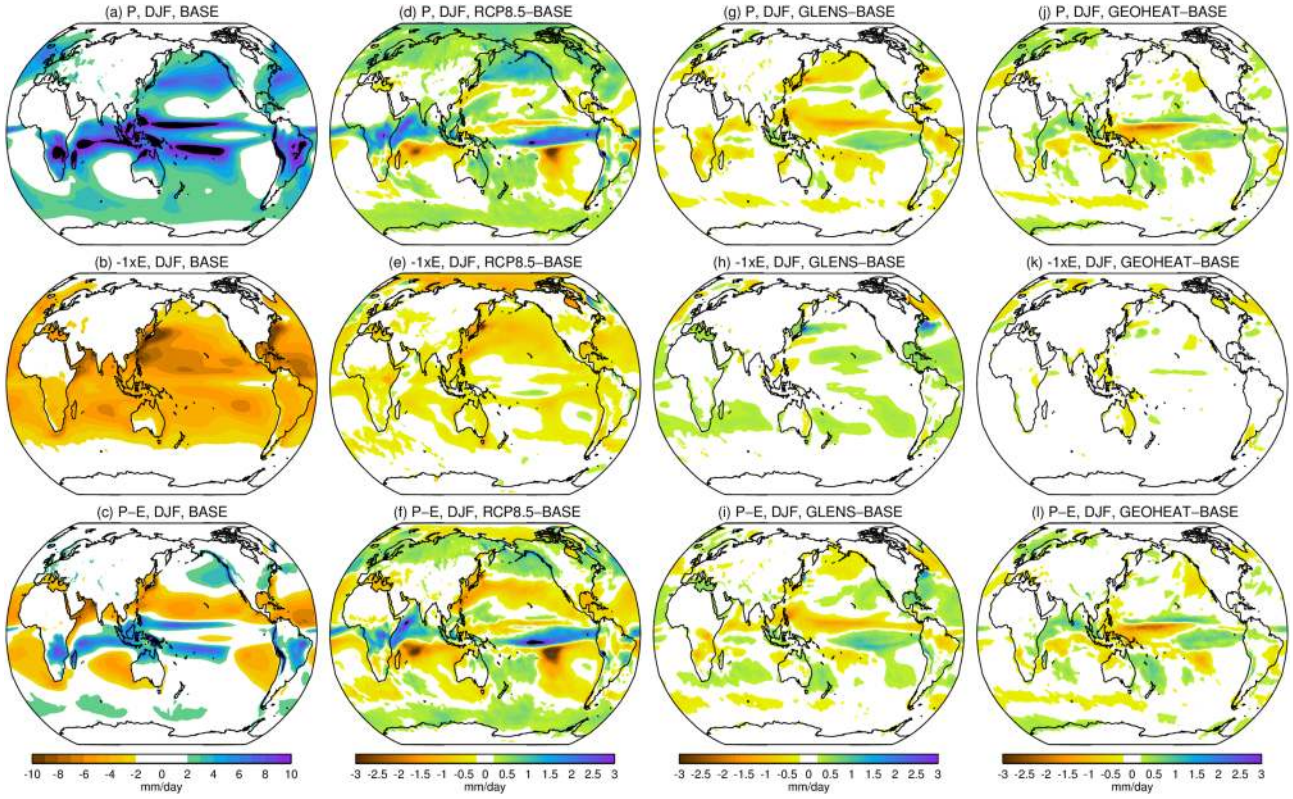

Figure 7. DJF averaged precipitation, −1× evaporation and precipitation−evaporation for BASE. (d)–(f)/(g)–(i)/(j)–(l) are as (a)–(c) but for RCP8.5−BASE, GLENS−BASE, and GEOHEAT−BASE. DJF = December-January-February, GLENS = Geoengineering Large Ensemble.

Despite all these possible reasons behind differences between GLENS and the GEOHEAT experiments, it is clear that stratospheric heating does play an important role and, in particular, results in a poleward shift of the midlatitude westerlies and a weakening of the tropical divergent circulation.

4. Hydroclimate Changes

4.1. A Global Overview

A global view of P, E and $P-E$ for the BASE climate, RCP8.5−BASE, GLENS−BASE, and GEOHEAT−BASE is provided in Figures 6 and 7 for JJA and DJF, respectively. The significance of these anomalies and the similarities and differences between GLENS and the stratospheric heating experiments (including GEOHEAT_S) will be discussed in more detail on a region by region basis below. In general, under RCP8.5 evaporation increases and, over most ocean areas, wet regions get wetter, dry regions get drier (Figures 6 and 7d–f). Over land and over the tropical Pacific, the pattern of $P-E$ does not conform to this wet-get-wetter, dry-get-drier pattern, as changes in circulation and relative humidity (Byrne & O'Gorman, 2015) or changes in SST patterns (Chadwick et al., 2013; Xie et al., 2010) play a role. With geoengineering, substantial regional hydroclimate changes also occur. Evaporation decreases (Figures 6 and 7h), as expected given the global energetic constraints discussed above. In addition, the general pattern of change in P and $P-E$ in the tropics is for wet regions to become drier and dry regions to become wetter (Panels g and i of Figures 6 and 7). The same is true in the annual mean and the other seasons (Figure S2).

With stratospheric heating alone, the reduction in evaporation is minimal over much of the globe (Figures 6 and 7k) as the global energetic balances have not been substantially perturbed. There are, however, precipitation changes that bear some similarity to the overall precipitation responses seen in GLENS (compare panels j and g in Figures 6 and 7) which will now be discussed in more detail on a region-by-region basis.

4.2. The Tropics

In JJA, the GLENS precipitation anomalies are significant over much of the tropical domain and are characterized by a wet-get-drier, dry-get-wetter pattern (Figure 8b). Most locations where precipitation exceeds 5 mm/day in BASE, exhibit a decline in P (red contour). This includes a reduction in a northwest to southeast

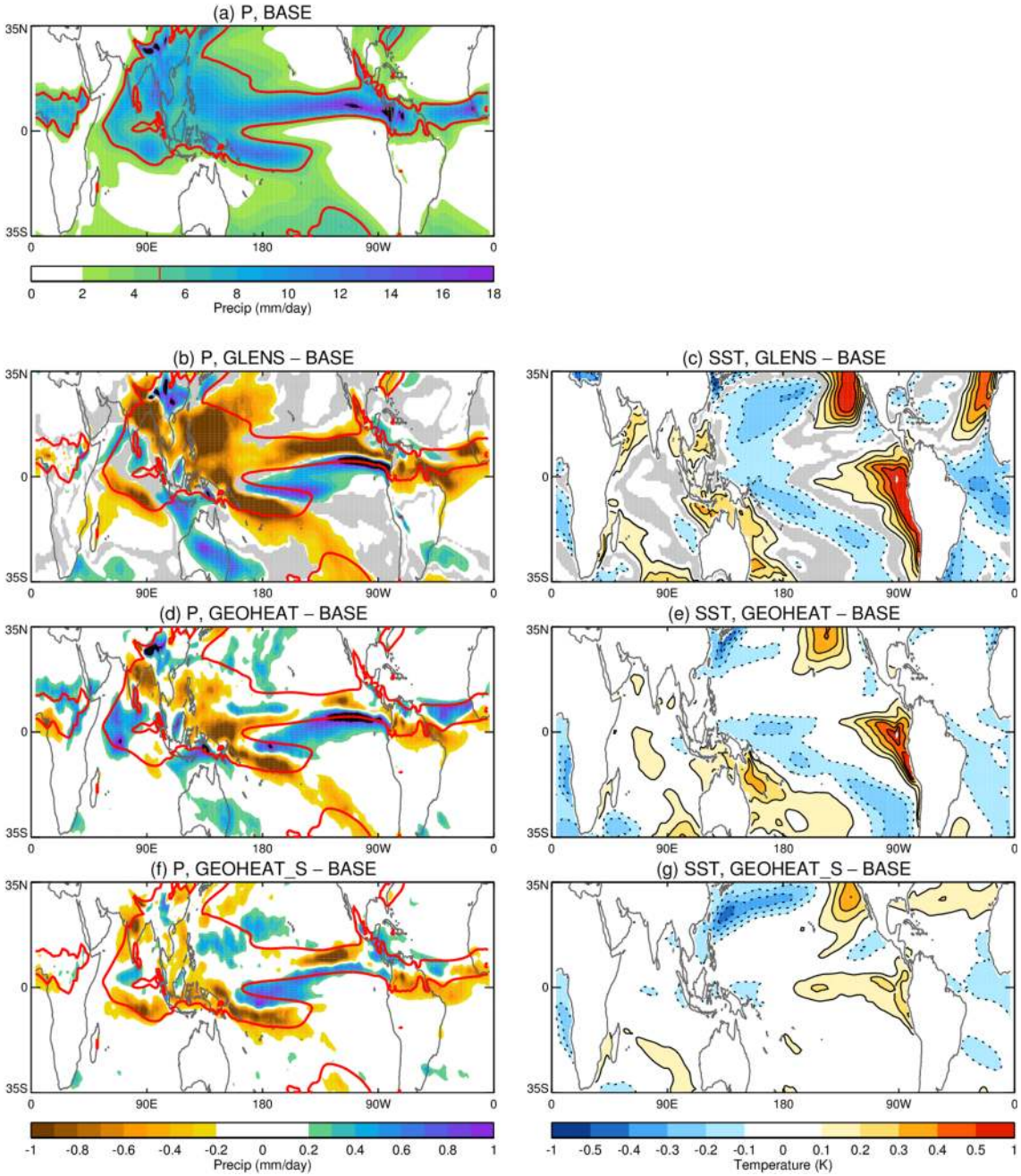

Figure 8. JJA averages. (a) BASE precipitation with the 5 mm/day contour highlighted in red. (b) GLENS−BASE precipitation. (c) GLENS−BASE SST anomalies from the zonal mean. Gray shading in (b) and (c) shows regions where the ensemble mean anomalies are not significantly different from zero at the 95% level by a one-sided *t*-test. (d)–(e) are as (b)–(c), but for GEOHEAT−BASE and (f)–(g) are as (b)–(c) but for GEOHEAT_S−BASE. Significance is not shown in (d)–(g) to allow the pattern to be seen clearly for comparison with (b) and (c), but the significance of anomalies over land will be assessed in subsequent figures. Note the nonlinear contour interval in the SST panels. GLENS = Geoengineering Large Ensemble, JJA = June-July-August.

strip from India into the South Pacific Convergence Zone, in the West Pacific and extending in a zonal strip along the northern portion of the ITCZ, and over the northern portion of South America and the tropical Atlantic. Regions that are characterized by climatologically low precipitation such as the eastern equatorial Pacific and Australia exhibit an increase. These *P* changes accompany the weakening of the tropical divergent circulation (Figure 4h) and a weakened east-west gradient in tropical Pacific SSTs (Figure 8c).

There is a striking similarity in the patterns of tropical JJA *P* and SST change between GLENS and GEOHEAT (compare Figures 8b and 8c with 8d and 8e). GEOHEAT also exhibits drying in a northwest-southeast

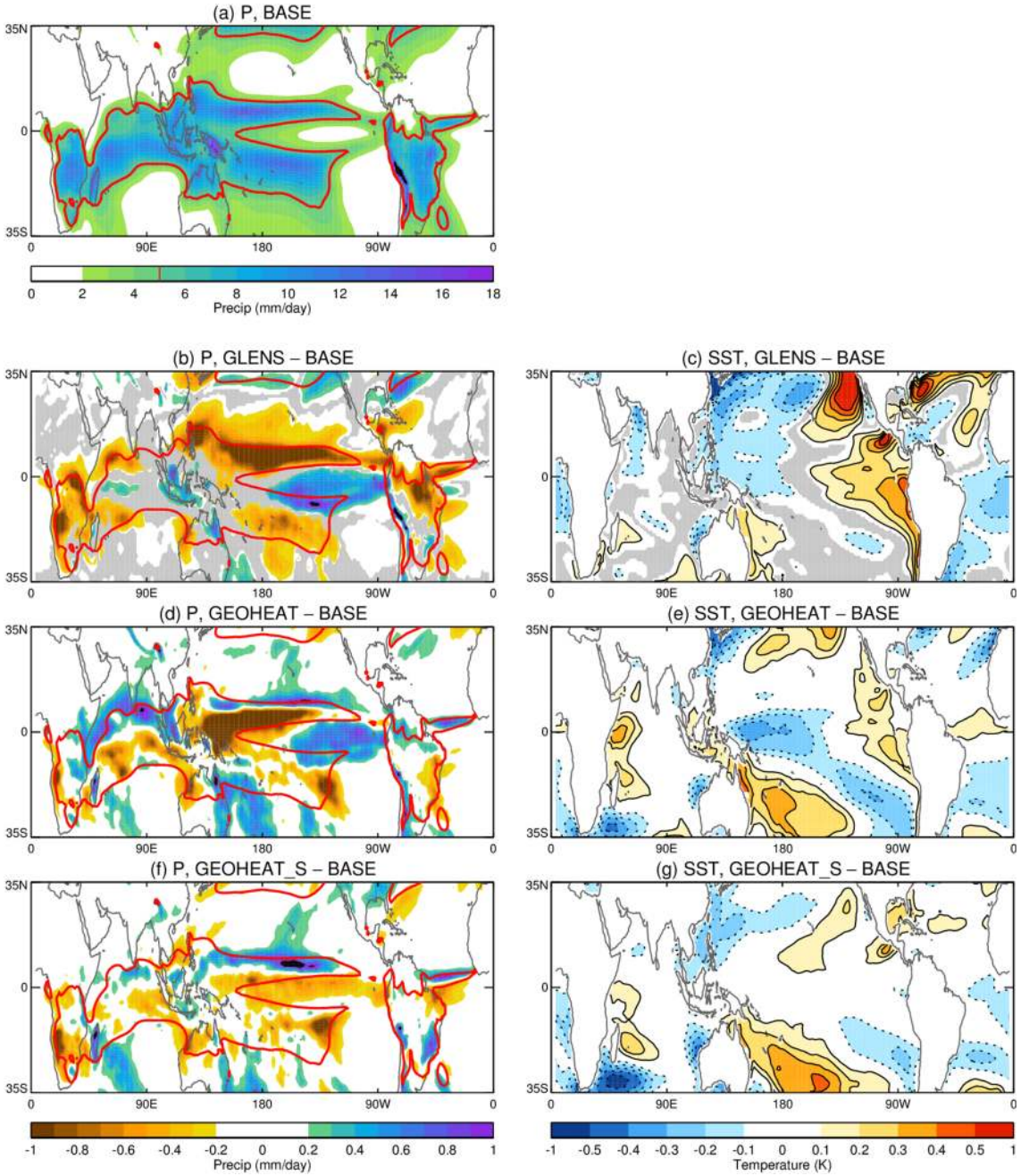

Figure 9. DJF averages. (a) BASE precipitation with the 5 mm/day contour highlighted in red. (b) GLENS−BASE precipitation. (c) GLENS−BASE SST anomalies from the zonal mean. Gray shading in (b) and (c) shows regions where the ensemble mean anomalies are not significantly different from zero at the 95% level by a one-sided *t*-test. (d)–(e) are as (b)–(c), but for GEOHEAT−BASE and (f)–(g) are as (b)–(c) but for GEOHEAT_S−BASE. Significance is not shown in (d)–(g) to allow the pattern to be seen clearly for comparison with (b) and (c), but the significance of anomalies over land will be assessed in subsequent figures. Note the nonlinear contour interval in the SST panels. DJF = December-January-February, GLENS = Geoengineering Large Ensemble.

strip from India into the South Pacific Convergence Zone, a wetting of the eastern tropical Pacific and drying over South America along with a weakening of the east-west gradient in tropical Pacific SSTs. The same is true for GEOHEAT_S, although the SST pattern has not had a chance to fully evolve yet, and as such, the precipitation increase in the far eastern equatorial Pacific and decline in the west is reduced.

In DJF, regions that are characterized by high *P* in BASE also tend to exhibit a decline in GLENS (Figure 9b), and there is an increase in *P* in the eastern tropical Pacific along with a reduction in the east-west gradient of SSTs. Again, a broadly similar pattern of *P* change is found in GEOHEAT (Figure 9d) in the tropical Pacific,

but it differs substantially from GLENS in the Indian ocean, the northern edge of the tropical Pacific, and over South America (Figure 9h). The tropical Pacific *P* changes are largely absent in GEOHEAT_S (Figure 9f) which is likely due to the fact that the reduced east-west gradient in tropical Pacific SSTs has not yet had a chance to form (Figure 9g).

Broadly, the tropospheric response to stratospheric heating consists of a wet-get-drier, dry-get-wetter pattern, which accompanies a weakening of the divergent circulation in the tropics. In the equatorial region of the Pacific, this weakening of the divergent circulation in the tropics is eventually also accompanied by a weakening of the east-west gradient in topical Pacific SSTs which leads to a further enhancement of the drying to the west and wetting to the east. An El Niño-like response to sulfate geoengineering and large volcanic eruptions have been found in previous studies (e.g., Khodri et al., 2017; Maher et al., 2015; Trisos et al., 2018). Khodri et al. (2017) argued for the important role of volcanic aerosol induced cooling over Africa for the El Niño-like signal in the year following volcanic eruptions. However, in the GEOHEAT experiments, the radiative influences of the aerosols on land temperatures are not present, and the similarity in tropical Pacific SST changes between GLENS and GEOHEAT suggests that the dynamical response to the warming of the lower stratosphere is an important contribution to the long-term SST changes found in this geoengineering scenario.

There are regional exceptions to the wet-get-drier, dry-get-wetter pattern, such as over China and the western Indian Ocean during JJA or the northern part of the Indian Ocean during DJF. We suspect these regional deviations arise in response to nonlocal circulation changes that accompany the precipitation and vertical motion responses elsewhere. As an example, the northern Indian Ocean during DJF is climatologically a wet region, but not as wet as to the south or east (Figure 9a). If the response to stratospheric heating in these wetter regions to the south and east dominates, the resulting changes in the divergent circulation may lead to an increased convergence in the northern Indian Ocean through mass conservation, thereby leading to enhanced precipitation and a deviation from the wet-get-drier, dry-get-wetter pattern. However, causality is difficult to disentangle since reduced precipitation will always be accompanied by reduced low level convergence and vice-versa, and it cannot be concluded that one is causing the other; they are simply consistent.

Notable features that are not captured by the stratospheric heating experiments are the drying to the east of the Philippines and the magnitude of the wetting over China and Australia. The stratospheric heating experiments would not be expected to exhibit all the tropical *P* changes found in GLENS. For one thing, the broad reductions in evaporation over the ocean basins do not happen in these experiments (Figures 6 and 7e vs. 7h and 7k), and so the accompanying changes to the moisture transports and associated moisture convergence and precipitation will not be present. This is a likely reason for the lack of drying in the region to the east of the Philippines. The direct radiative influence of GHGs on the magnitude of vertical motions and precipitation patterns (Bony et al., 2013) is also not present. But the fact that many of the features of the GLENS tropical *P* change occur in the stratospheric heating experiments suggests an important role for the response to stratospheric heating in setting up regional precipitation (and SST) changes in the tropics. This is also true for March-April-May (MAM) and September-October-November (SON) (Figure S2).

4.3. The Asian Summer Monsoon

For Asia, we focus only on the summer monsoon season (JJA) when the climatological precipitation is large, as is the response in GLENS. If warming under rising GHGs was allowed to continue, CESM1(WACCM) suggests that *P* would increase by 10–20% over much of Asia by the end of the 21st century (Figure 10b), and this is broadly in agreement with the CMIP5 ensemble mean (Figure 10c). The CMIP5 ensemble mean is, however, an average over considerable diversity. For example, averaged over India, the CMIP5 *P* change ranges from a decrease of 0.40 mm/day to an increase of 1.51 mm/day. The CESM1(WACCM) change of around 0.96 mm/day is well within the CMIP5 spread but lies on the wetter side.

If GHG-driven warming was offset with this form of geoengineering, GLENS suggests precipitation would decline over much of India, while it would increase over China and much of the Maritime continent (Figure 10d). Averaged over the whole of India, the ensemble mean reduction in *P* is 8.5% (0.53 mm/day) and, while evaporation is also reduced, the overall reduction in $P - E$ is 9.9% (0.34 mm/day; Figure 10g), which can be compared with the RCP8.5 increases in *P* and $P - E$ of 15.3% (0.95 mm/day) and 20.8% (0.72 mm/day), respectively. This reduction in summer $P - E$ leads to a reduction in soil moisture which reaches around 3.5% averaged over the whole of India in July (Figure 10i). See Cheng et al. (2019) for a more detailed

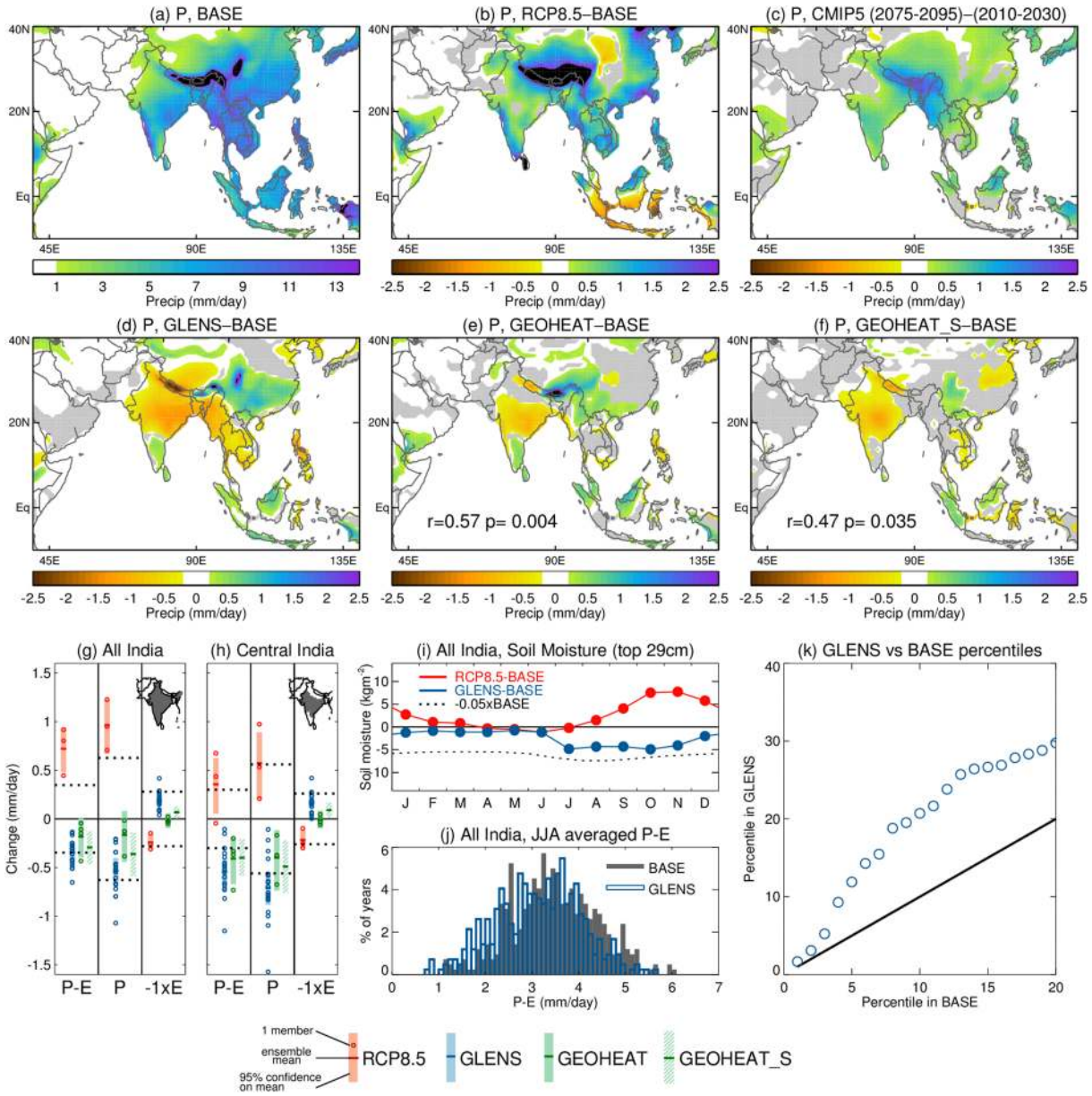

Figure 10. JJA averaged hydroclimate changes with a focus on Asian land regions. (a) BASE precipitation climatology, (b) Community Earth System Model Version 1(Whole Atmosphere Community Climate Model) RCP8.5−BASE, (c) CMIP5 RCP8.5 (2075-2095)-(2010-2030), (d) GLENS−BASE, (e) GEOHEAT−BASE, and (f) GEOHEAT_S−BASE precipitation anomalies. Gray shading in (b) and (d)–(f) depicts regions that are not significantly different from zero by the bootstrapping test outlined in section 2.2, and in (c), it depicts regions where fewer than 2/3 of the models agree on the sign of the change. In (e) and (f), the quoted correlation is the pattern correlation with the GLENS response (panel d) over the land regions in the domain shown, and the p value is determined by the bootstrapping methodology outlined in section 2.2. (g) Area averaged $P - E$, P, and $-1 \times E$ anomalies over India (gray region in inset) for each Community Earth System Model Version 1(Whole Atmosphere Community Climate Model) experiment. Horizontal dotted lines show ±10% of the BASE climatology. (h) As (g) but averaged over the central portion of India (gray region in inset), bounded in the northwest,northeast,southwest,and southeast by the states of Rajasthan, West Bengal, Maharashtra, and Andhra Pradesh. (i) Monthly soil moisture anomalies for RCP8.5−BASE and GLENS−BASE averaged over the whole of India. Black dotted line shows −5% of the BASE climatology. (j) Probability Distribution Function (PDF) of yearly JJA averaged $P - E$ averaged over the whole of India for BASE and GLENS. (k) For the percentiles of the BASE distribution (x-axis), we show the percentile of the GLENS distribution at which the same value of JJA averaged $P - E$ occurs (blue circles). If there were no change to the distribution, these should fall on the 1:1 line (black line). If the blue circles lie above the 1:1 line, then it indicates that $P - E$ values at this low end of the BASE distribution occur more frequently in GLENS. For example, the value of around 12 (y-axis) at the 5th percentile (x-axis) indicates that JJA averaged $P - E$ lower than the 5th percentile of BASE, occurs around 12% of the time in GLENS. DJF = December-January-February, GLENS = Geoengineering Large Ensemble, JJA = June-July-August, RCP8.5 = Representative Concentration Pathway 8.5.

analysis of soil moisture changes in GLENS. CESM1(WACCM) does exhibit a dry bias over India and a wet bias over China (Figure S1c) which may impact on the magnitude of these changes, but we suspect it would not qualitatively change the results.

Averaged over central India where the reduction of P in GLENS is most severe, the ensemble mean P and $P-E$ in GLENS declines by 12.7% (0.71 mm/day) and 18.1% (0.54 mm/day), respectively (Figure 10h). This can be compared with the RCP8.5 increases of 10.2% (0.57 mm/day) and 11.9% (0.36 mm/day). The spread of the ensemble members, however, shows that the combination of the forced response and internal variability can produce a wide range of anomalies in $P-E$ over a 20-year average, ranging from a reduction of only 3.6% (0.11 mm/day) in one member to a reduction of 38.4% (3.54 mm/day) in another over central India (Figure 10h).

The population of India relies heavily on the summer monsoon rains for agriculture. Individual monsoon failures can, therefore, have severe socio-economic impacts. Considering the area average over the whole of India, under geoengineering in GLENS, the whole distribution of JJA averaged $P-E$ shifts toward drier values (Figure 10j). As a result, the probability of extreme dry years, as defined by any percentile of the BASE distribution between around the 5th and 20th, is roughly doubled in GLENS compared to BASE (Figure 10k). This change is very well reproduced if the BASE distribution is simply shifted by the mean difference in $P-E$ between GLENS and BASE (not shown). That is, the mean reduction in $P-E$ in GLENS makes monsoon failures become roughly twice as likely, compared to BASE, while in RCP8.5 the overall increase in precipitation reduces the likelihood of monsoon failures (not shown). That being said, the increase in precipitation that is projected to occur under RCP8.5 could have its own detrimental effects such as increasing the likelihood of flooding. A rigorous evaluation of the benefits and risks associated with geoengineering would require a detailed impact assessment of both these possible futures.

The pattern of precipitation change in the stratospheric heating experiments is very similar to the full GLENS response (compare Figures 10e and 10f with 10d) with significant pattern correlations of 0.57 or 0.47 between GLENS and GEOHEAT or GEOHEAT_S, respectively. Over central India, at least half of the precipitation response in GLENS arises through stratospheric heating alone (Figure 10h), and in fact, the GLENS and GEOHEAT precipitation responses are not statistically distinguishable from each other with the present sample sizes (Figure 10h or see supporting information, Figure S5 for the difference plot in map form). The large uncertainty due to internal variability makes it difficult to quantify, with more certainty, the proportion of precipitation reduction that arises from stratospheric heating alone. But the GEOHEAT experiments indicate that stratospheric heating is likely an important contributor to the precipitation changes that arise during JJA over the domain in Figure 10 and to the drying of central India in particular.

To summarize, while previous studies have shown a reduction in precipitation over India in model experiments of geoengineering, both in the contexts of solar dimming (Tilmes et al., 2013) and sulfate aerosol injections (Robock, 2008), here the larger ensemble allows for a quantification of the behavior of the tails of the distribution of seasonal average precipitation. In addition, the fact that stratospheric heating alone can produce a substantial fraction of the drying over India suggests that the drying that occurs in solar dimming experiments may not be for entirely the same reasons. Under reduced incoming solar radiation, a logical argument could be made for cooling of the summertime land leading to a weakening of the land-sea temperature contrast and, therefore, a weakening of the monsoon. However, this argument would not explain the response to stratospheric heating in isolation, and therefore, another mechanism, whereby stratospheric heating dynamically induces a precipitation reduction over India, must play a role.

4.4. South America

In the JJA season, CESM1(WACCM) and the CMIP5 models suggest that, under RCP8.5, precipitation will decline over Amazonia and the central portion of Chile (Figures 11b and 11c). This is also true under geoengineering (Figure 11d) and comparison of Figures 11d, 11e, and 11f makes clear that the response to stratospheric heating is a dominant contribution to this. Averaged over Amazonia, the JJA GLENS precipitation decline of just under 10% is reproduced with imposed stratospheric heating alone (compare the P anomalies with the black dashed line in Figure 11m left). This is despite the fact that the elevated CO_2 influence on plant physiology effects, which has been argued could be an important driver of drying over the Amazon (Richardson et al., 2018), is absent. Over the whole continent, the pattern correlations between GEOHEAT or GEOHEAT_S and GLENS are 0.71 or 0.78 (p <0.001). The JJA precipitation reduction over Patagonia of just under 7% is also reproduced in response to the stratospheric heating (Figure 11n). This is

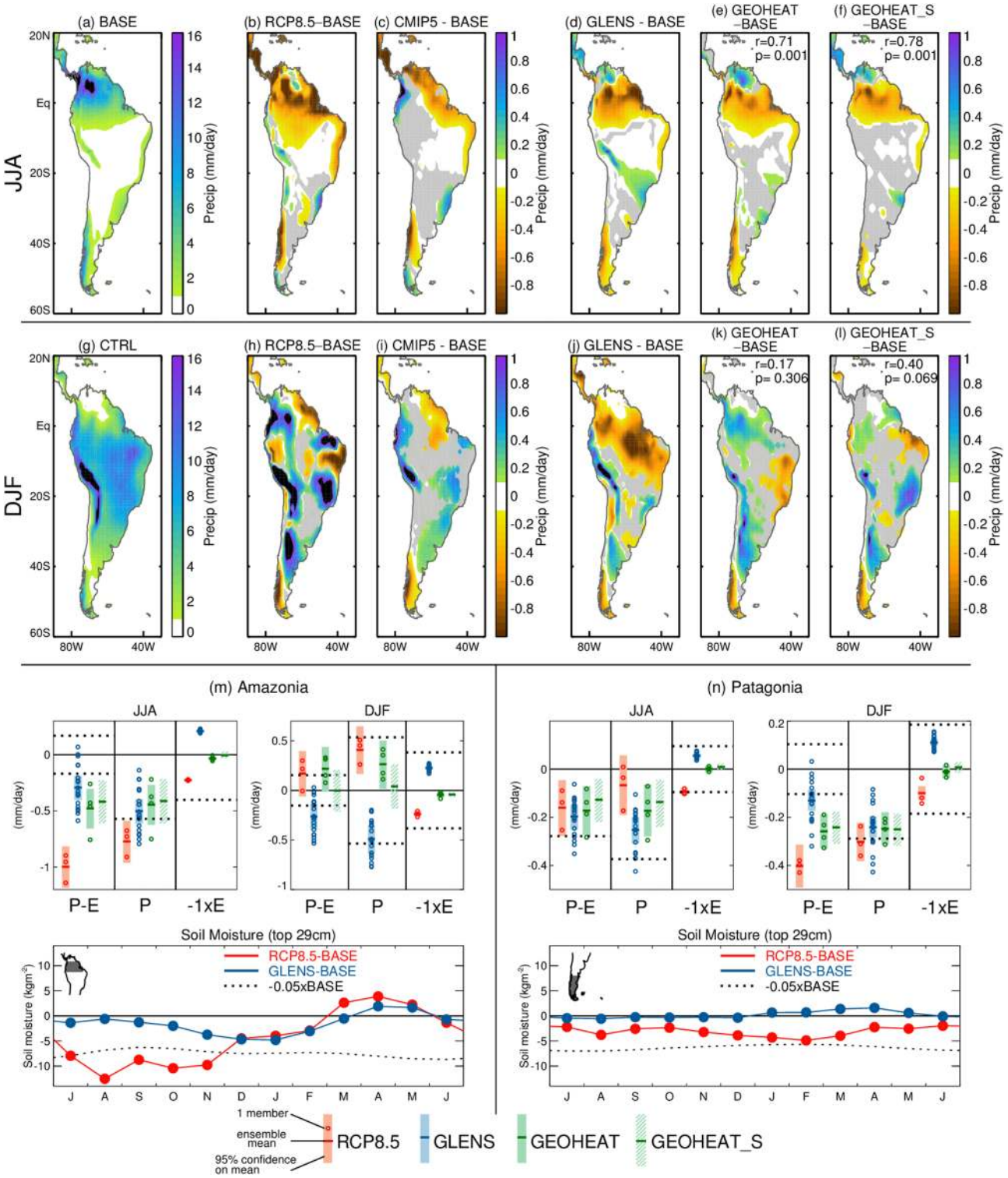

Figure 11. (a)–(f) South American Precipitation in JJA: (a) BASE, (b) RCP8.5−BASE, (c) CMIP5 RCP8.5 (2075-2095)−(2010-2030), (d) GLENS−BASE, (e) GEOHEAT−BASE, (f) GEOHEAT_S−BASE. (g)–(l) as (a)–(f) but for DJF. In (e)/(f) and (k)/(l), the quoted correlation is the pattern correlation with the GLENS response (d)/(j) over the domain shown, and the *p* value is determined by the bootstrapping methodology outlined in section 2.2. (m) shows hydroclimate changes averaged over Amazonia (land regions between 5^{o}S and 5^{o}N, see bottom panel inset, gray region) with the top panels showing *P*, *E* and *P* − *E* for (left) JJA and (right) DJF and the bottom panel showing soil moisture anomalies. Horizontal dotted lines in the top panels show ±10% of the BASE climatology (when that occurs within the plot range) while the horizontal dotted line in the bottom panel shows -5% of the BASE climatology. (n) is as (m) but averaged over Patagonia, defined as land regions poleward of 42^{o}S (gray region in bottom panel inset). Colors in (m) and (n) are defined in the legend. DJF = December-January-February, GLENS = Geoengineering Large Ensemble, JJA = June-July-August, RCP8.5 = Representative Concentration Pathway 8.5.

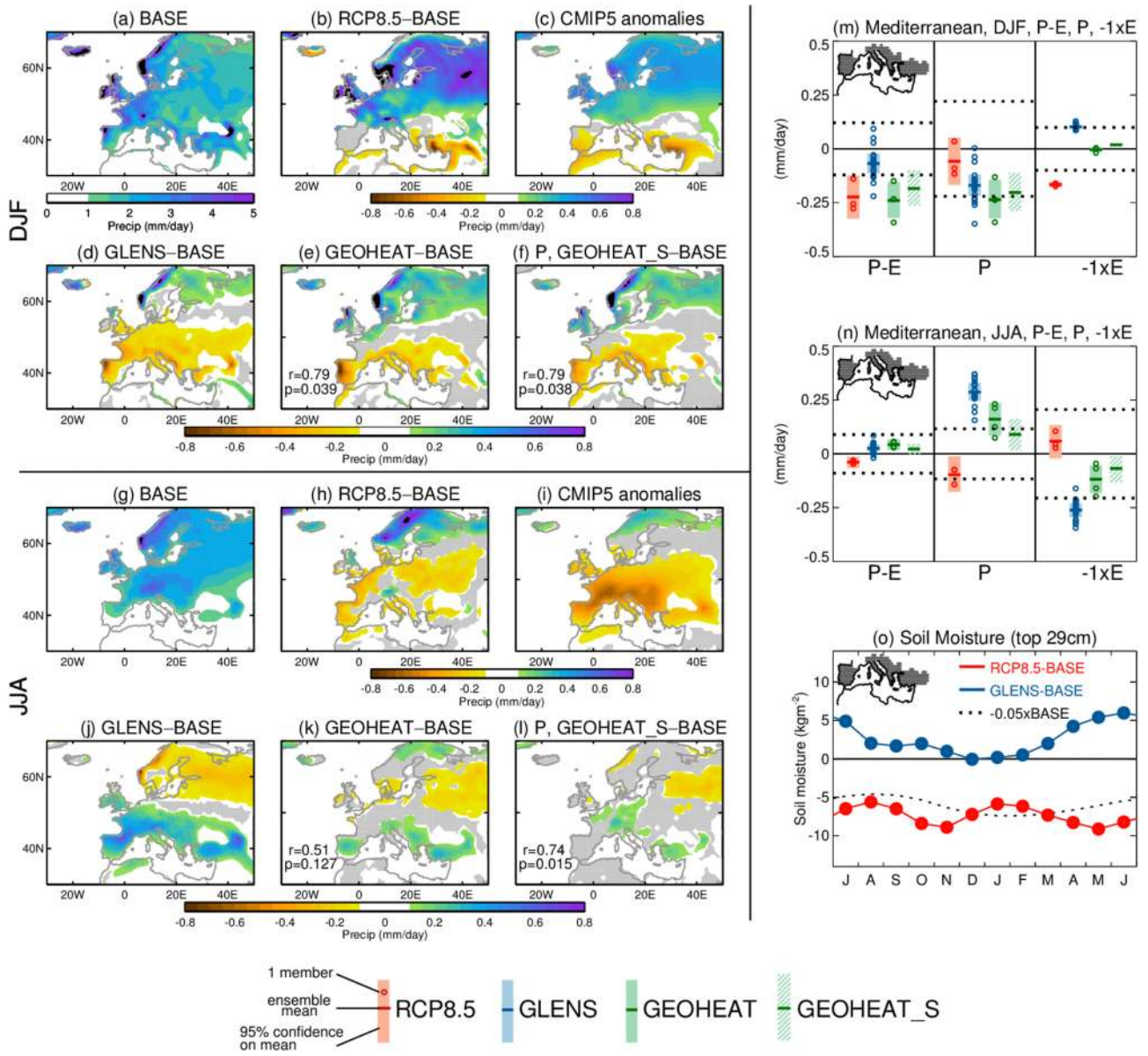

Figure 12. (a)–(f)/(g)–(l) Precipitation changes over the Mediterranean and Europe during DJF/JJA. (m)–(o) show the regional averages over Mediterranean countries from Spain and Portugal in the west to Turkey in the east (grey inset in the panels). This region was chosen as it is a region that is vulnerable to climate change under RCP8.5 and is a region where there is a wintertime reduction in precipitation in GLENS. France is omitted from this Mediterranean average as only a small portion of France exhibits drying. (m) shows P, $-1 \times E$ and $P - E$ for DJF, and (n) shows the equivalent for JJA. Colors are defined in the legend. (o) shows monthly soil moisture in the top 29 cm of soil. DJF = December-January-February, GLENS = Geoengineering Large Ensemble, JJA = June-July-August, RCP8.5 = Representative Concentration Pathway 8.5.

despite the fact that the transient eddy activity weakens considerably more in GLENS than in the heating experiments (Figures 4e and 4f). Transient eddy fluxes of moisture are actually not an important contribution to this change as the reduced precipitation on the west coast of this region is associated with reduced near surface zonal flow impinging on the Andes (supporting information, Fig S6 and Text S1)—a feature that is well reproduced with stratospheric heating alone (Figures 4b and 4c).

In DJF, over Amazonia, the precipitation changes in RCP8.5 are more complicated (Figures 11h and 11i). In GLENS, there is a projected drying over much of the region (Figure 11j), but unlike for JJA, there is no correspondence between the GLENS response and that induced by the stratospheric heating, and the responses in GEOHEAT and GEOHEAT_S do not look similar to each other either (Figures 11k and 11l). In contrast, in the southern portion of South America, the precipitation changes are, again, well reproduced by

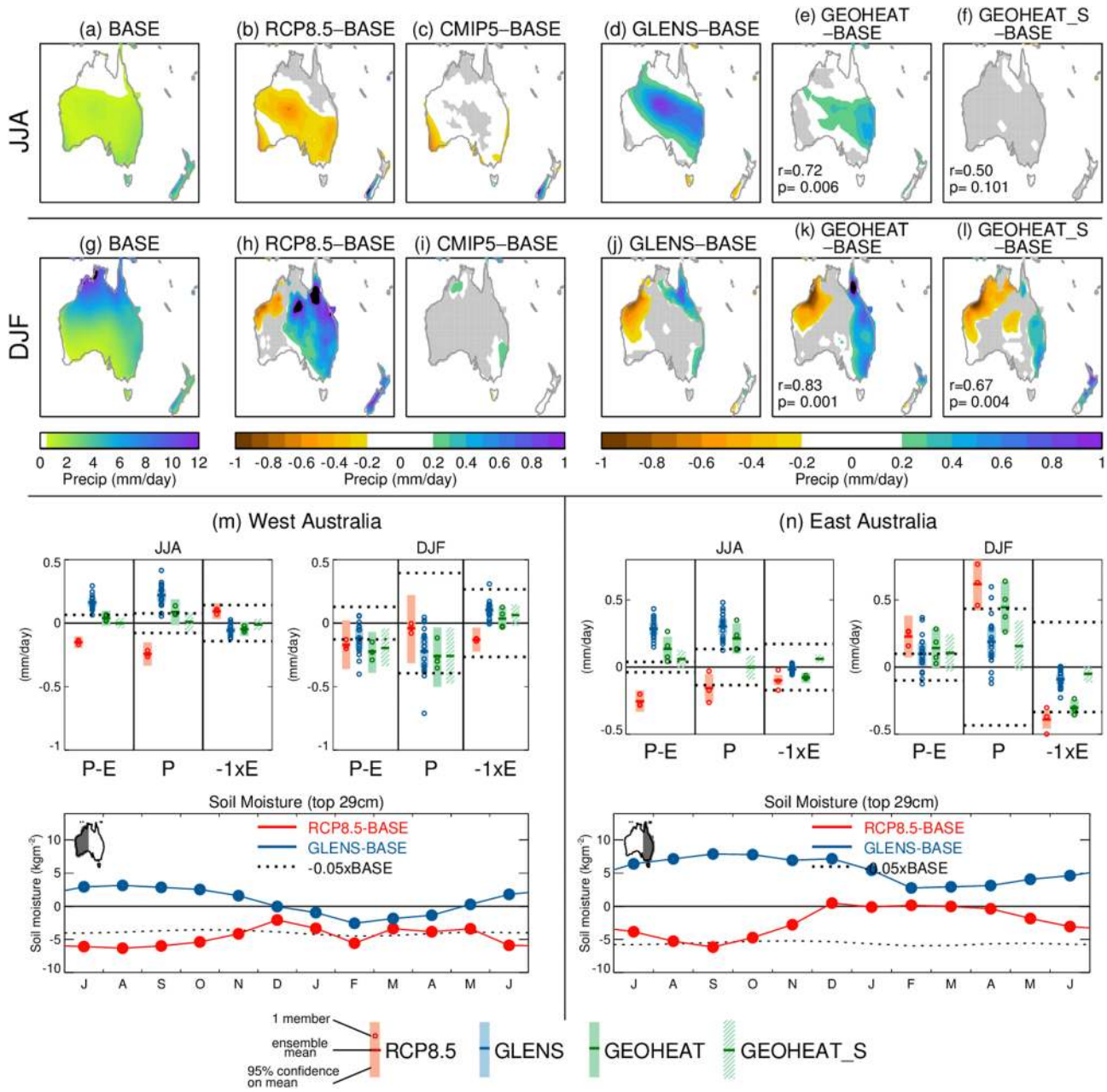

Figure 13. As Figure 11 but for Australia and with a regional focus on western (west of 130°E) and eastern (east of 140°E) Australia in (m) and (n). DJF = December-January-February, GLENS = Geoengineering Large Ensemble, JJA = June-July-August, RCP8.5 = Representative Concentration Pathway 8.5.

the stratospheric heating alone and relate to the reduced zonal flow impinging on the Andes in this region which occurs in the presence of stratospheric heating alone (Figures 5b and 5c).

Even though substantial precipitation anomalies occur in GLENS, much greater soil moisture changes occur in RCP8.5. Over Amazonia, the far greater reduction in $P - E$ during JJA in RCP8.5 results in a far greater drying of the soil that is found in GLENS. The same is true for Patagonia where soil moisture remains roughly at BASE values in GLENS but declines over the whole year in RCP8.5 with a maximum reduction of almost 5% in late summer (Figure 11n). So, while precipitation changes for South America in GLENS are of comparable magnitude to those in RCP8.5, the impacts in terms of soil aridification are likely to be greater under RCP8.5.

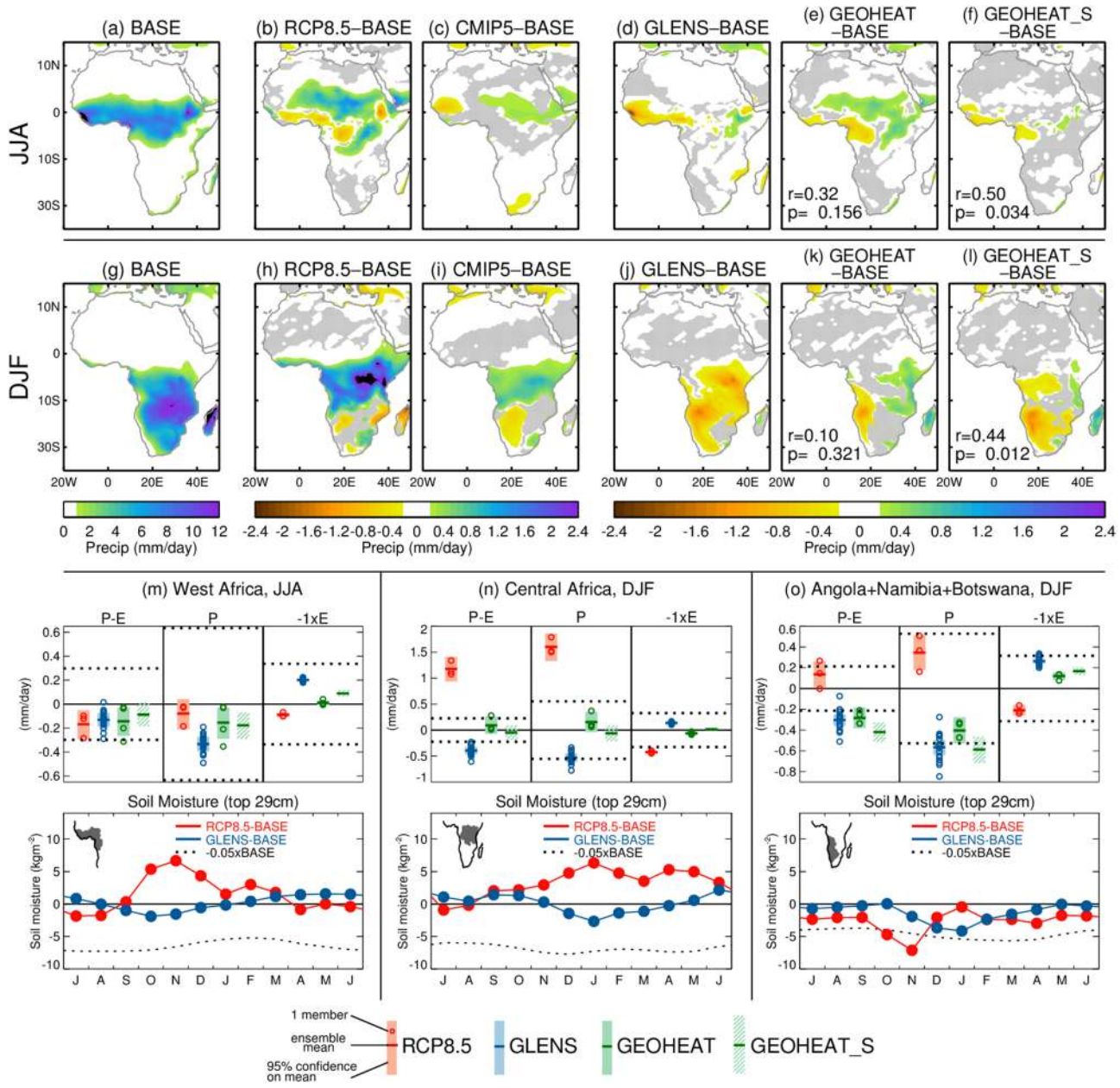

Figure 14. As Figure 11 but for Africa. The region of focus in panel (m) is the coastal countries around the Gulf of Guinea from Guinea in the west to the Republic of Congo in the south and east, and the top panel shows the JJA season where this region exhibits reduced precipitation in GLENS. The region of focus in panel (n) is central Africa (Democratic Republic of Congo, Tanzania, Rwanda, Burundi, Uganda and Kenya), and the top panel shows the DJF season when this region exhibits reduced precipitation. The region of focus in panel (o) is the average over Angola, Namibia, and Botswana, and the top panel shows DJF, when this region exhibits reduced precipitation. In (m–o), the gray region on the inset map on the bottom panel shows the averaging region.
DJF = December-January-February, GLENS = Geoengineering Large Ensemble, JJA = June-July-August, RCP8.5 = Representative Concentration Pathway 8.5.

4.5. Europe and the Mediterranean

The Mediterranean is considered a climate change hot-spot (Giorgi, 2006) and is expected to dry considerably over the coming decades (Seager et al., 2014). During winter (DJF), the CMIP5 models and CESM1(WACCM) predict a decline in precipitation under RCP8.5 (Figures 12b and 12c). When coupled with a large increase in evaporation, the net result is a reduction in $P-E$ of 18.5% in the CESM1(WACCM) ensemble mean, averaged over the Mediterranean region (Figure 12m). Under sulfate geoengineering, the reduction in precipitation in the Mediterranean is actually greater than under RCP8.5, but because evaporation is also reduced, as opposed to increased, the reduction in $P-E$ is less (only 5.6%, Figure 12m). Stratospheric heating is a dominant contributor to the GLENS DJF P reduction over the Mediterranean as well as the P increase to the North

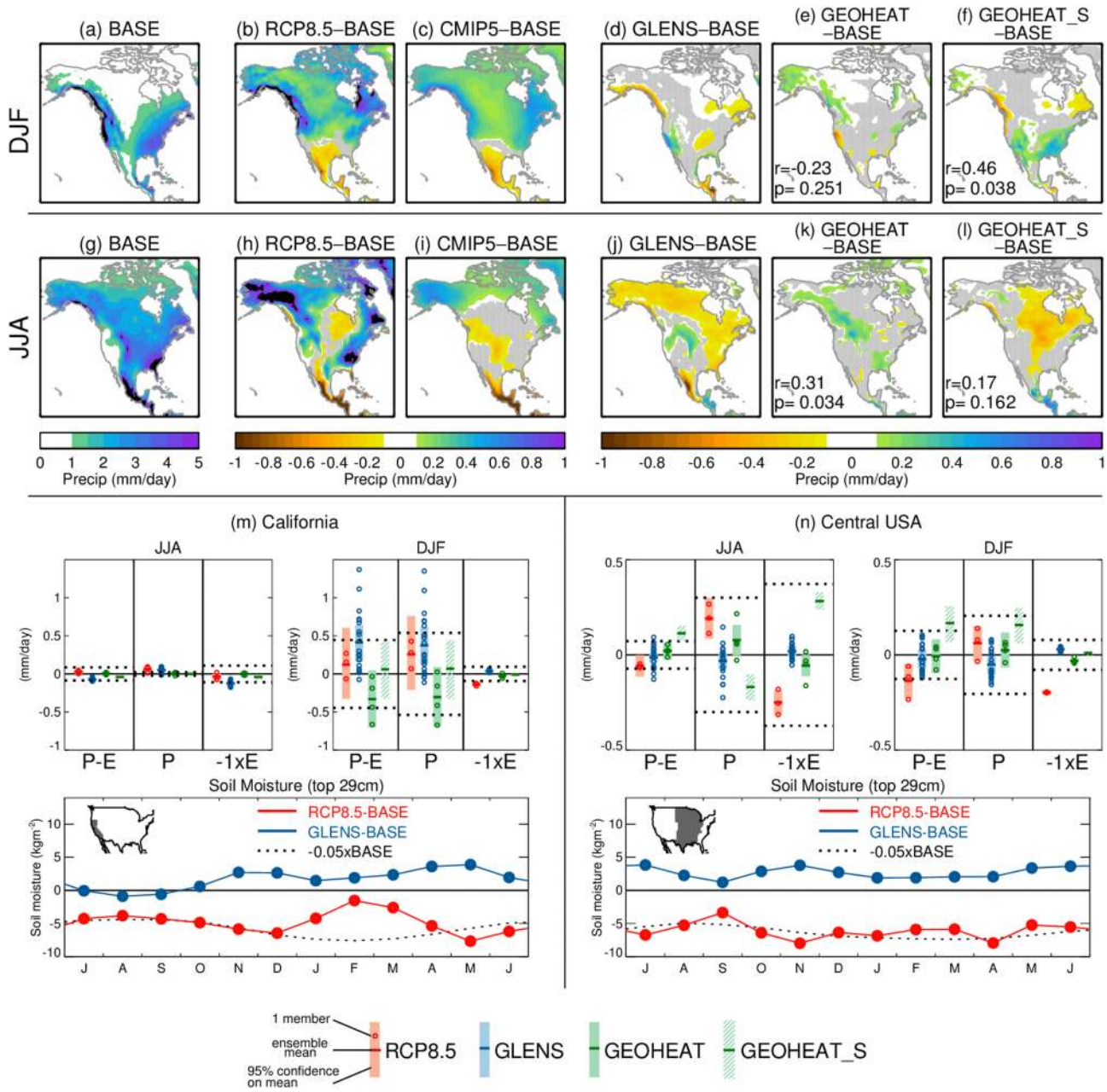

Figure 15. (a)–(f)/(g)–(l) Precipitation changes over North America during DJF/JJA. (m) and (n) show changes over regions of agricultural importance for the USA: California (m) and the central USA bounded by North Dakota, Ohio, Texas, and Alabama (n). Colors are defined in the legend. DJF = December-January-February, GLENS = Geoengineering Large Ensemble, JJA = June-July-August, RCP8.5 = Representative Concentration Pathway 8.5.

over Scandinavia and western Russia (Figures 12e, 12f, and 12m). This may at first seem surprising given the far greater reduction in storm track activity over Europe found in GLENS than in GEOHEAT (Figures 5e and 5f) but can be reconciled by the fact that the Mediterranean drying and Scandinavian wetting is actually associated with altered mean flow moisture flux convergence that accompanies the poleward shift of the Atlantic westerlies (supporting information, Figure S7), and this change in the westerlies is comparable between GLENS and GEOHEAT. The difference in storm track intensity between GLENS and GEOHEAT is responsible for the slightly different structures of the precipitation patterns over Europe in DJF. The weaker storm track in GLENS results in a drying over central Europe (Figure S7), and this is presumably reduced in GEOHEAT where the storm track activity weakens less.

Under RCP8.5, precipitation also declines in JJA (Figure 12h), but in GLENS, the JJA *P* change actually consists of an increase over the Mediterranean and a decrease to the North (Figure 12g). The accompanying JJA increase in soil moisture more than compensates for the drying that occurs in DJF, such that Mediterranean soil moisture does not decrease at any time of the year in GLENS (Figure 12o), which is in contrast to the year round soil moisture reduction of around 5% that occurs in RCP8.5. At least a portion of the summertime precipitation change in GLENS is associated with stratospheric heating (Figures 12k and 12l).

4.6. Other Regions: Australia, Africa, and North America

Here we briefly summarize some key features of the responses found in Australia, Africa, and North America, depicted in Figures 13, 14, and 15.

- **Australia:** In JJA, GLENS geoengineering more than compensates for the drying that is projected under RCP8.5 (Figure 13b) and results in an increase in precipitation (Figure 13d). A portion of this increase occurs in GEOHEAT as a result of the stratospheric influence combined with the subsequent SST evolution (Figure 13e). In DJF, the importance of the stratospheric heating influence in the GLENS response is also clear (Figure 13j–l) as this gives rise to a precipitation reduction in the west and increase in the east that very closely resembles the full GLENS response. In terms of soil moisture impacts, soil moisture is projected to decrease over much of the year in RCP8.5 while it mostly increases in GLENS (Figure 13m and 13n, bottom).
- **Africa:** Geoengineering results in a reduction in precipitation over most regions with climatologically high precipitation in Africa such as western equatorial Africa in JJA (Figure 14d) and regions south of the equator in DJF (Figure 14j). Whether stratospheric heating plays an important role in these responses is regionally dependent. In particular, the DJF reduction in *P* over Angola, Namibia, and Botswana in GEOHEAT is close to that seen in the full GLENS (10.7%/0.57 mm/day in the GLENS ensemble mean and 7.6%/0.4 mm/day in the GEOHEAT ensemble mean (Figure 14o, top)). However, to the north east of here, stratospheric heating results in an increase in *P*, while GLENS exhibits a decrease. In terms of soil moisture, precipitation increases lead to an increase in soil moisture under RCP8.5 in equatorial Africa, which does not happen in GLENS where soil moisture does not change dramatically (Figures 14m and 14n). Over Angola, Namibia, and Botswana, there is a seasonal dependence as to whether GLENS exhibits more or less soil moisture reduction than RCP8.5 (Figure 14o).
- **North America:** During DJF under continued warming, precipitation is projected to increase over much of the continent, with the exception of a drying of the interior southwest of the United States and Mexico (Seager et al., 2014; and Figures 15b and 15c). In GLENS, precipitation changes are minimal in DJF, limited to patchy regions of reduced *P* in the east and a wetting on the southwest coast and a drying to the north of that, which accompanies the equatorward shift of the Pacific westerlies in this season (Figure 5b). In JJA, the *P* changes in GLENS are generally opposite to those under RCP8.5 with a reduction in *P* over much of the north and east and an increase in the central and western United States. There is no resemblance between the response to stratospheric heating and the full GLENS here, which is not surprising given their differences in Pacific circulation change (Figure 5b vs. Figure 5c). Over California, reduced precipitation in the spring and autumn (not shown, Swain et al., 2018), together with enhanced evapotranspiration in a warmer climate (Cook et al., 2015), lead to a reduction in soil moisture throughout the year under RCP8.5 (Figure 15m). The enhanced evaporation under RCP8.5 also leads to a desiccation of the soil by around 5% over the central United States (Figure 15n). In both California and the central Unites States, this is more than compensated for in GLENS where soil moisture increases slightly (Figures 15m and 15n).

5. Discussion

Throughout this analysis, we have focused on a severe geoengineering scenario: The geoengineering is used to fully offset the almost 4K of global warming that occurs under RCP8.5 forcing by 2075–2095. Our reasoning behind this is that it provides a larger signal-to-noise ratio than would be possible with more moderate scenarios and, therefore, allows us to more easily detect, and quantify the role of stratospheric heating. If geoengineering were to be implemented, it has been advocated (Keith & MacMartin, 2015) that it should only be used to temporarily or partially ameliorate the effects of GHG warming while other, more permanent, mitigation strategies are developed (Tilmes et al., 2016). In Figure 16, the scaling of the precipitation response to geoengineering as a function of the amount of global warming that is being offset can be assessed for various land regions and seasons where geoengineering was found, in the previous sections, to result in

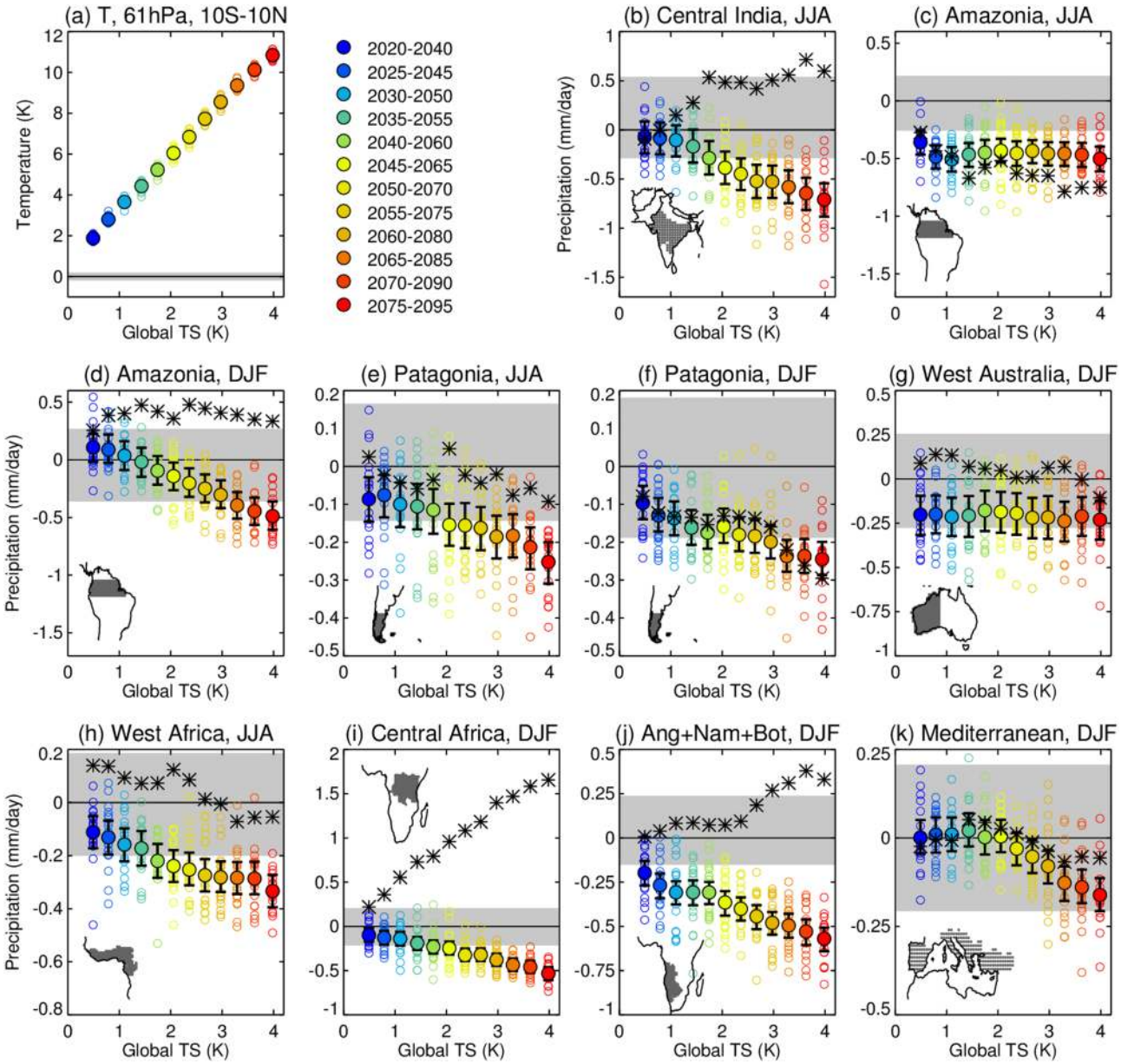

Figure 16. Precipitation anomalies as a function of the annual mean globally averaged temperature anomalies (RCP8.5−BASE) that are being offset by geoengineering (*x*-axis) for 20-year climatologies between 2020 and 2095 separated at 5-year intervals (blue to red colors for GLENS). Filled circles show the ensemble mean GLENS−BASE difference, and the black error bars show the 90% confidence interval on the ensemble mean anomaly (5th–95th percentile range). Open circles show the anomalies from BASE for each individual GLENS member, and black asterisks show the ensemble mean anomalies under RCP8.5. Gray shading shows the mininum to maximum range of the anomaly of each individual BASE member from the BASE ensemble mean, that is, the range of uncertainty on a 20-year climatology within the BASE climate. (a) Zonal mean annual mean stratospheric temperature anomalies averaged from 5°S-5°N at 61.5 hPa, which is the pressure of the model level nearest the temperature anomaly maximum. (b)–(k) show precipitation anomalies over the various regions that exhibit substantial drying in GLENS as discussed in sections 4.3–4.6. Inset maps in (b)–(k) show the area used for averaging.
DJF = December-January-February, GLENS = Geoengineering Large Ensemble, JJA = June-July-August, RCP8.5 = Representative Concentration Pathway 8.5.

a precipitation decline. For the majority of the regions, the ensemble mean precipitation response (filled circles) scales roughly linearly with the degree of global warming that is being offset (MacMartin et al., 2019). Importantly, this is true for central India which was the one region where, in terms of soil moisture, the GLENS scenario would be viewed as considerably worse than continued global warming. The analysis of these experiments from one model indicates that in the period 2030–2050, at which point only 1K of global warming is being offset, there is only a 4 in 20 chance that over a 20-year period, the average precipitation

would be outside of that of 20-year climatologies that have been experienced before for central India (compare unfilled circles with gray shading in Figure 16b). Increase this to a 2K global warming offset, however, and the model suggests that it is a near certainty that a 20-year average under these conditions would be drier than climatology and about a 15/20 chance that it would be drier than ever previously experienced. In each of these regions, the wide range of precipitation responses among the ensemble members (open circles) indicates the challenges involved in detecting the true magnitude of the geoengineering influence locally if it were to be implemented in the real world (MacMartin et al., 2019) and demonstrates that the risks and benefits of geoengineering should be quantified by consideration of the full probability distribution of outcomes that could result from both the forced response and internal variability.

There are three notable exceptions to the above discussed linearity: Amazonia during JJA (Figure 16c), West Australia during DJF (Figure 16g), and the Mediterranean during DJF (Figure 16k). Amazonia in JJA and West Australia in DJF were two regions where stratospheric heating was found to explain the full precipitation decline, and in these regions, the precipitation response does not scale at all linearly with global warming offset. The response appears almost immediately with the anomalies during 2020–2040 being rather similar to those during 2075–2095. This is despite the fact that the degree of stratospheric warming scales linearly with the degree of global warming offset (Figure 16a). This is a rather curious finding that requires further explanation through an improved mechanistic understanding. Why this should be the case for these regions, but not for other tropical regions where stratospheric heating plays an important role (e.g., central India) is currently unclear. In contrast, for the Mediterranean during DJF, the precipitation decline is not apparent until more than 2K of global warming is being offset, suggesting that this response may not be realized if only a moderate geoengineering scenario was implemented.

Delineating the relative role of the stratospheric heating is useful for a variety of reasons. First, the fact that it was found to play an important role in various features of the response (in agreement with Ferraro et al., 2014), calls into question the relevance of results of solar dimming experiments for quantification of the impacts of stratospheric sulfate geoengineering. Second, perhaps one of the biggest uncertainties in sulfate geoengineering is the radiative properties of the stratospheric aerosols, given that this depends on complex microphysical processes. The fact that stratospheric heating was found to play an important role in the climate response motivates an improved understanding of this and a narrowing down of that particular uncertainty. Third, it raises the possibility that the hydroclimate response could be reduced if aerosol compositions that absorb less or scatter more than sulfate were used (Keith et al., 2016). Finally, this represents a first step toward a full mechanistic understanding of the processes that give rise to precipitation changes under sulfate geoengineering and motivates further analysis to understand how stratospheric heating has the influence it does. This mechanistic understanding is crucial to determine the extent to which models are trustworthy in their representation of the relevant processes.

Much remains to be understood about the mechanisms that give rise to the precipitation response to stratospheric heating, particularly in the tropics. Various mechanisms have been proposed, whereby lower stratospheric heating results in reduced precipitation in regions of deep tropical convection, primarily in the contexts of the response to the quasi biennial oscillation. Arguments have been put forth whereby changes in lower stratospheric stability or vertical wind shear influence the upper reaches of convection (Giorgetta et al., 1999; Gray et al., 1992), or whereby lower stratospheric warming exerts its influence through changes in upper level clouds and associated column integrated radiative heating (Nie & Sobel, 2015). Ferraro et al. (2014) argue that sulfate geoengineering influences tropical precipitation through upper tropospheric warming and associated stability change arising from both the thermal emissions from the sulfate aerosols and from the warmer lower stratosphere. In our experiments, the aerosols themselves are not present, so if this mechanism is at work, it would have to arise from the warmer lower statosphere alone.

The GEOHEAT experiments suggest that a leading order effect of the stratospheric heating in the tropics is to reduce precipitation in regions of climatologically high precipitation and increase it elsewhere. In other words, the response is a wet-get-drier, dry-get-wetter pattern. That being said, there are a number of regional exceptions to this rule, particularly during DJF. To bolster the conclusion that the leading order effect of stratospheric heating is to make wet regions drier and dry regions wetter, we show preliminary results with an idealized CESM aquaplanet configuration using the same model physics as GLENS (Medeiros et al., 2016; Figure 17). This configuration is run under perpetual equinox conditions with prescribed SSTs following the "control" profile of (Neale & Hoskins, 2001) plus an idealized zonal asymmetry in the tropics intended to

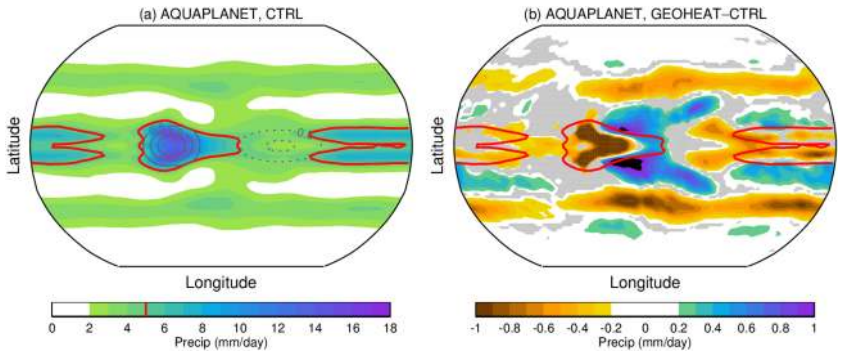

Figure 17. Prescribed SST aquaplanet experiments with Community Earth System Model Version 1 with the Community Atmosphere Model (CAM5) as its atmospheric component (CESM1(CAM5)). Thirty-year climatologies are shown. (a) Shading = precipitation, red contour = the 5 mm/day precipitation contour, and gray contours = prescribed SST deviations from the zonal mean with a contour interval of 0.5K and the 0 contour omitted (solid = positive, dashed = negative). (b) The difference in precipitation between a stratospheric heating experiment and control where the same stratospheric heating perturbation as in GEOHEAT has been imposed. Gray shading indicates regions where the anomalies are not significantly different from zero at the 95% level by a two sided *t*-test.

mimic the warm pool-cold tongue region (gray contours in Figure 17a). When the same stratospheric heating as in GEOHEAT is imposed, the regions characterized by climatologically high precipitation in the tropics (roughly within the red 5 mm/day contour) exhibit a precipitation decline, while elsewhere, the precipitation increases (Figure 17b). This indicates that the wet-get-drier, dry-get-wetter pattern is (a) independent of Earth's continental geometry, SST distribution, and the presence of land, (b) occurs in the absence of a seasonal cycle, and (c) occurs in the absence of any changes to surface temperatures, which are fixed in this experiment. This indicates that understanding of the leading order changes in GEOHEAT can be obtained by understanding the direct atmospheric circulation and precipitation response to stratospheric heating in an idealized setting without any of these features. Investigations are currently under way using this idealized framework as a test-bed to distinguish between the various mechanisms described above and to assess the sensitivity to the stratospheric heating profile.

The primary limitation of the comparison between GLENS and GEOHEAT and GEOHEAT_S is that we have implicitly assumed that the stratospheric heating would have the same influence if it were imposed within a climate where CO_2 has increased and incoming solar irradiance has decreased, that is, we have assumed that the contributions from stratospheric heating and those from the other components of combined GHG increase and geoengineering add up linearly. Future experiments are planned to test this assumption.

6. Conclusion

To conclude, the GLENS experiments have demonstrated that substantial precipitation changes occur in regions of the tropics and midlatitudes when global warming is offset by sulfate geoengineering. Complementary experiments, in which stratospheric heating is imposed in isolation, indicate an important role for the dynamical response to stratospheric heating in many aspects of this response. Stratospheric heating generally leads to a wet-get-drier, dry-get-wetter pattern in the tropics and is implicated in drying over India and Amazonia during JJA. Stratospheric heating also acts to force a poleward shifting of the westerlies in the SH and in the North Atlantic during DJF, leading to drying over southwestern South America throughout the year and the Mediterranean during winter. Despite substantial precipitation changes, over much of the globe, the impacts of global warming in terms of soil moisture aridification are largely ameliorated by the geoengineering. India is the primary exception to this. The precipitation decline in the summer monsoon more than offsets reduced evaporation, resulting in an overall reduction in soil moisture. GLENS suggests that failures of the Indian summer monsoon would be twice as likely as in present day, if geoengineering were used to fully offset the warming forced by the RCP8.5 scenario by 2075–2095. This response does, however, scale linearly with the degree of global warming that is being offset, and so this impact would be considerably reduced if a more moderate geoengineering scenario was to be followed. Details of the regional hydroclimate response will also depend on the geoengineering strategy employed. For example, experiments with CESM1(WACCM) in which only equatorial injection was used and interhemispheric temperature gradients were not maintained, actually exhibit an increase in precipitation over India during JJA Kravitz et al.

(2019 their Fig. 9b). This is likely because, in addition to the forcings experienced in GLENS, the changes in interhemispheric temperature gradients can induce hemispheric scale shifts in the regions of tropical convergence around the equator.

As with all modeling studies, these results comes with the caveat that the extent to which they are relevant for the real world depends on the reliability of the representation of the relevant processes within the model. Quantitatively, the precipitation biases present in CESM1(WACCM; Figure S1) may impact on the changes seen, but we suspect will not qualitatively alter conclusions. Nevertheless, comparable experiments with other models would be of use to assess the robustness of the conclusions drawn here. A crucial next step is to understand the mechanisms responsible for the changes found. Here we have isolated the role of stratospheric heating. Stratospheric heating is found to be important which motivates an improved understanding of the mechanisms involved in that pathway of the response. Work is currently underway to address this and to distinguish between the various mechanisms that have been proposed in the literature such as the role of altered cloud radiative effects (Nie & Sobel, 2015), the role of stability changes and their influence on convection (Giorgetta et al., 1999; Gray et al., 1992), or other, yet to be determined, mechanisms.

Acknowledgments
The CESM project is supported primarily by the National Science Foundation (NSF). This material is based upon work supported by the National Center for Atmospheric Research, which is a major facility sponsored by the National Science Foundation under Cooperative Agreement 1852977. Computing and data storage resources, including the Cheyenne supercomputer (doi:10.5065/D6RX99HX), were provided by the Computational and Information Systems Laboratory (CISL) at NCAR. We acknowledge the World Climate Research Programme's Working Group on Coupled Modelling, which is responsible for CMIP, and we thank the climate modeling groups (listed in Table S1) for producing and making available their model output. For CMIP, the U.S. Department of Energy's Program for Climate Model Diagnosis and Intercomparison provides coordinating support and led development of software infrastructure in partnership with the Global Organization for Earth System Science Portals. Support for B. K. was provided in part by the National Science Foundation through agreement CBET-1931641, the Indiana University Environmental Resilience Institute, and the *Prepared for Environmental Change* Grand Challenge initiative. The Pacific Northwest National Laboratory is operated for the U.S. Department of Energy by Battelle Memorial Institute under contract DE-AC05-76RL01830. All CMIP5 data used in this study are available from the Earth System Grid (https://cmip.llnl.gov/cmip5/data_portal.html). All CESM1(WACCM) simulations are available via the Earth System Grid (see information at www.cesm.ucar.edu/projects/community-projects/GLENS/) and the DOI for the GLENS simulations is DOI 10.5065/D6JH3JXX.

References

Ammann, C. M., Washington, W. M., Meehl, G. A., Buja, L., & Teng, H. (2010). Climate engineering through artificial enhancement of natural forcings: Magnitudes and implied consequences. *Journal of Geophysical Research*, *115*, D22109. https://doi.org/10.1029/2009JD012878

Andrews, T., Forster, P. M., & Gregory, J. M. (2009). A surface energy perspective on climate change. *Journal of Climate*, *22*(10), 2557–2570. https://doi.org/10.1175/2008JCLI2759.1

Bala, G., Caldeira, K., & Nemani, R. (2010). Fast versus slow response in climate change: Implications for the global hydrological cycle. *Climate Dynamics*, *35*(2-3), 423–434. https://doi.org/10.1007/s00382-009-0583-y

Bala, G., Duffy, P. B., & Taylor, K. E. (2008). Impact of geoengineering schemes on the global hydrological cycle. *PNAS*, *105*(22), 7664–7669. https://doi.org/10.1073/pnas.0711648105

Baldwin, M. P., & Dunkerton, T. J. (2001). Stratospheric harbingers of anomalous weather regimes. *Science*, *294*(5542), 581–584. https://doi.org/10.1126/science.1063315

Blackstock, J., Battisti, D., Caldeira, K., Eardley, D., Katz, J., Keith, D., et al. (2009). Climate engineering responses to climate emergencies. *Novim*. https://arxiv.org/pdf/0907.5140.pdf

Bony, S., Bellon, G., Klocke, D., Sherwood, S., Fermepin, S., & Denvil, S. (2013). Robust direct effect of carbon dioxide on tropical circulation and regional precipitation. *Nature Geoscience*, *6*, 447–451. https://doi.org/10.1038/ngeo1799

Budyko, M. I. (1977). *Climatic changes* (p. 244). Washington DC: American Geophysical Society. https://doi.org/10.1029/SP010

Byrne, M. P., & O'Gorman, P. A. (2015). The response of precipitation minus evapotranspiration to climate warming: Why the "wet-get-wetter, dry-get-drier" scaling does not hold over land. *Journal of Climate*, *28*(20), 8078–8092. https://doi.org/10.1175/JCLI-D-15-0369.1

Chadwick, R., Boutle, I., & Martin, G. (2013). Spatial patterns of precipitation change in CMIP5: Why the rich do not get richer in the tropics. *Journal of Climate*, *26*(11), 3803–3822. https://doi.org/10.1175/JCLI-D-12-00543.1

Cheng, W., MacMartin, D. G., Dagon, K., Kravitz, B., Tilmes, S., Richter, J. H., et al. (2019). Soil moisture and other hydrological changes in a stratospheric aerosol geoengineering large ensemble. *Journal of Geophysical Research: Atmospheres*, *124*. https://doi.org/10.1029/2018JD030237

Cook, B. I., Ault, T. R., & Smerdon, J. E. (2015). Unprecendented 21st century drought risk in the American southwest and Central Plains. *Science Advances*, *1*(1), e1400082. https://doi.org/10.1126/sciadv.1400082

Crutzen, P. J. (2006). Albedo enhancement by stratospheric sulfur injections: A contribution to resolve a policy dilemma? *Climatic Change*, *77*(3-4), 211–220. https://doi.org/10.1007/s10584-006-9101-y

DallaSanta, K., Gerber, E. P., & Toohey, M. (2019). The circulation response to volcanic eruptions: The key roles of stratospheric warming and eddy interactions. *Journal of Climate*, *32*(4), 1101–1120. https://doi.org/10.1175/JCLI-D-18-0099.1

Dinh, T., & Fueglistaler, S. (2017). Mechanism of fast atmospheric energetic equilibration following radiative forcing by CO_2. *Journal of Advances in Modeling Earth Systems*, *9*, 2468–2482. https://doi.org/10.1002/2017MS001116

Fasullo, J. T., Tilmes, S., Richter, J. H., Kravitz, B., MacMartin, D. G., Mills, M. J., & Simpson, I. R. (2018). Persistent polar ocean warming in a strategically geoengineered climate. *Nature Geoscience*, *11*(12), 910–914. https://doi.org/10.1038/s41561-018-0249-7

Ferraro, A. J., Charlton-Perez, A. J., & Highwood, E. J. (2013). Stratospheric dynamics and midlatitude jets under geoengineering with space mirrors and sulfate and titania aerosols. *Journal of Geophysical Research: Atmospheres*, *120*, 414–429. https://doi.org/10.1002/2014JD022734

Ferraro, A. J., Highwood, E. J., & Charlton-Perez, A. J. (2011). Stratospheric heating by potential geoengineering aerosols. *Geophysical Research Letters*, *38*, L24706. https://doi.org/10.1029/2011GL049761

Ferraro, A. J., Highwood, E. J., & Charlton-Perez, A. J. (2014). Weakened tropical circulation and reduced precipitation in response to geoengineering. *Environmental Research Letters*, *9*(1), 014001. https://doi.org/10.1088/1748-9326/9/1/014001

Forster, P. M. d. F., & Shine, K. P. (1999). Stratospheric water vapour changes as a possible contributor to observed stratospheric cooling. *Geophysical Research Letters*, *26*(21), 3309–3312. https://doi.org/10.1029/1999GL010487

Forster, P. M. d. F., & Shine, K. P. (2002). Assessing the climate impact of trends in stratospheric water vapor. *Geophysical Research Letters*, *29*(6), 1086. https://doi.org/10.1029/2001GL013909

Fyfe, J. C., Cole, J. N. S., Arora, V. K., & Scinocca, J. F. (2013). Biogeochemical carbon coupling influences global precipitation in geoengineering experiments. *Geophysical Research Letters*, *40*, 651–655. https://doi.org/10.1002/GRL.50166

Giorgetta, M. A., Bengtsson, L., & Arpe, K. (1999). An investigation of QBO signals in the east Asian and Indian monsoon in GCM experiments. *Climate Dynamics*, *15*(6), 435–450. https://doi.org/10.1007/s003820050292

Giorgi, F. (2006). Climate change hot-spots. *Geophysical Research Letters*, *33*, L08707. https://doi.org/10.1029/2006GL025734

Govindasamy, B., & Caldeira, K. (2000). Geoengineering earth's radiation balance to mitigate co_2-induced climate change. *Geophysical Research Letters*, *27*(14), 2141–2144. https://doi.org/10.1029/1999GL006086

Gray, W. M., Sheaffer, J. D., & Knaff, J. A. (1992). Hypothesized mechanism for stratospheric QBO influence on ENSO variability. *Geophysical Research Letters*, *19*(2), 107–110. https://doi.org/10.1029/91GL02950

Haigh, J. D., Blackburn, M., & Day, R. (2005). The response of tropospheric circulation to perturbations in lower-stratospheric temperature. *Journal of Climate*, *18*(17), 3672–3685. https://doi.org/10.1175/JCLI3472.1

Heckendorn, P., Weisenstein, D., Fueglistaler, S., Luo, B. P., Rozanov, E., Schraner, M., et al. (2009). The impact of geoengineering aerosols on stratospheric temperature and ozone. *Environmental Research Letters*, *4*(4), 045108. https://doi.org/10.1088/1748-9326/4/4/045108

Hurrell, J. W., Holland, M. M., Gent, P. R., Ghan, S., Kay, J. E., Kushner, P. J., et al. (2013). The community earth system model: A framework for collaborative research. *Bulletin of the American Meteorological Society*, *94*(9), 1339–1360. https://doi.org/10.1175/BAMS-D-12-00121.1

Iles, C. E., & Hegerl, G. C. (2015). Systematic change in global patterns of streamflow following volcanic eruptions. *Nature Geoscience*, *8*(11), 838–842. https://doi.org/10.1038/ngeo2545

IPCC (2013). Book section SPM. In *Summary for Policymakers* (pp. 1–30). Cambridge, United Kingdom and New York, NY, USA: Cambridge University Press. https://doi.org/10.1017/CBO9781107415324.004

Irvine, P., Emanuel, K., He, J., Horowitz, L. W., Vecchi, G., & Keith, D. (2019). Halving warming with idealized solar geoengineering moderates key climate hazards. *Nature Climate Change*, *9*(4), 295–299. https://doi.org/10.1038/s41558-019-0398-8

Jones, A., Haywood, J., Boucher, O., Kravitz, B., & Robock, A. (2010). Geoengineering by stratospheric SO_2 injections: Results from the met Office HadGEM2 climate model and comparison with the Goddard institute for space studies model. *Atmospheric Chemistry and Physics*, *10*(13), 5999–6006. https://doi.org/10.5194/acp-10-5999-2010

Jones, A., Haywood, J. M., Alterskjaer, K., Boucher, O., Cole, J. N. S., Curry, C. L., et al. (2013). The impact of abrupt suspension of solar radiation management (termination effect) in experiment G2 of the Geoengineering model Intercomparison project (GeoMIP). *Journal of Geophysical Research: Atmospeheres*, *118*, 9743–9752. https://doi.org/10.1002/jgrd.50762

Kalidindi, S., Bala, G., Modak, A., & Caldeira, K. (2015). Modeling of solar radiation management: A comparison of simulations using reduced solar constant and stratospheric sulphate aerosols. *Climate Dynamics*, *44*(9-10), 2909–2925. https://doi.org/10.1007/s00382-014-2240-3

Keith, D. W. (2000). Geoengineering the climate: History and prospect. *Annual Review of Energy and the Environment*, *25*(1), 245–284. https://doi.org/10.1146/annurev.energy.25.1.245

Keith, D. W., & MacMartin, D. G. (2015). A temporary, moderate and responsive scenario for solar geoengineering. *Nature Climate Change*, *5*(3), 201–206. https://doi.org/10.1038/nclimate2493

Keith, D. W., Weisenstein, D. K., Dykema, J. A., & Keutsch, F. N. (2016). Stratospheric solar geoengineering without ozone loss. *PNAS*, *113*(52), 14,910–14,914. https://doi.org/10.1073/pnas.1615572113

Khodri, M., Izumo, T., Vialard, J., Janicot, S., Cassou, C., Lengaigne, M., et al. (2017). Tropical explosive volcanic eruptions can trigger El Niño by cooling tropical Africa. *Nature Communications*, *8*(1), 778. https://doi.org/10.1038/s41467-017-00755-6

Kravitz, B., Caldeira, K., Boucher, O., Robock, A., Rasch, P. J., Alterskjaer, K., et al. (2013). Climate model response from the Geoengineering model Intercomparison project (GeoMIP). *Journal of Geophysical Research: Atmospheres*, *118*, 8320–8332. https://doi.org/10.1002/jgrd.50646

Kravitz, B., MacMartin, D. G., Mills, M. J., Richter, J. H., Tilmes, S., Lamarque, J.-F., et al. (2017). First simulations of designing stratospheric sulfate aerosol geoengineering to meet multiple simultaneous climate objectives. *Journal of Geophysical Research: Atmospheres*, *122*, 12,616–12,634. https://doi.org/10.1002/2017JD026874

Kravitz, B., MacMartin, D. G., Tilmes, S., Richter, J. H., Mills, M. J., Cheng, W., et al. (2019). Comparing surface and stratospheric impacts of geoengineering with different SO_2 injection strategies. *Journal of Geophysical Research: Atmospheres*, *124*, 7900–7918. https://doi.org/10.1029/2019JD030329

Kravitz, B., MacMartin, D. G., Wang, H., & Rasch, P. J. (2016). Geoengineering as a design problem. *Earth System Dynamics*, *7*(2), 469–497. https://doi.org/10.5194/esd-7-469-2016

Kravitz, B., Rasch, P. J., Forster, P. M., Andrews, T., Cole, J. N. D., Irvine, P. J., et al. (2013). An energetic perspective on hydrological cycle changes in the Geoengineering model Intercomparison project. *Journal of Geophysical Research: Atmospheres*, *118*, 13,087–13,102. https://doi.org/10.1002/2013JD020502

Kravitz, B., Robock, A., Forster, P. M., Haywood, J. M., Lawrence, M. G., & Schmidt, H. (2013). An overview of the Geoengineering model Intercomparison project (GeoMIP). *Journal of Geophysical Research: Atmospheres*, *118*, 13,103–13,107. https://doi.org/10.1002/2013JD020569

Liu, X., Easter, R. C., Ghan, S. J., Zaveri, R., Rasch, P., Shi, X., et al. (2012). Toward a minimal representation of aerosols in climate models: Description and evaluation in the community atmosphere model CAM5. *Geoscientific Model Development*, *5*(3), 709–739. https://doi.org/10.5194/gmd-5-709-2012

MacMartin, D. G., Kravitz, B., Keith, D. W., & Jarvis, A. (2014). Dynamics of the coupled human-climate system resulting from closed-loop control of solar geoengineering. *Climate Dynamics*, *43*(1-2), 243–258. https://doi.org/10.1007/s00382-013-1822-9

MacMartin, D. G., Wang, W., Kravitz, B., Tilmes, S., Richter, J. H., & Mills, M. J. (2019). Timescale for detecting the climate response to stratospheric aerosol geoengineering. *Journal of Geophysical Research: Atmospheres*, *124*, 1233–1247. https://doi.org/10.1029/2018JD028906

Maher, N., McGregor, S., England, M. H., & Sen Gupta, A. (2015). Effects of volcanism on tropical variability. *Geophysical Research Letters*, *42*, 6024–6033. https://doi.org/10.1002/2015GL064751

Manabe, S., & Wetherald, R. T. (1967). Thermal equilibrium of the atmosphere with a given distribution of relative humidity. *Journal of the Atmospheric Sciences*, *24*(3), 241–259. https://doi.org/10.1175/1520-0469(1967)024<0241:TEOTAW>2.0.CO;2

Maycock, A. C., Shine, K. P., & Joshi, M. M. (2011). The temperature response to stratospheric water vapour changes. *Quarterly Journal of the Royal Meteorological Society*, *137*(657), 1070–1082. https://doi.org/10.1002/qj.822

Mills, M. J., Richter, J. H., Tilmes, S., Kravitz, B., MacMartin, D. G., Glanville, A. A., et al. (2017). Radiative and chemical response to interactive stratospheric sulfate aerosols in fully coupled CESM1(WACCM). *Journal of Geophysical Research: Atmospheres*, *122*, 13,061–13,078. https://doi.org/10.1002/2017JD027006

Muri, H., Tjiputra, J., Ottera, O. H., Adakudlu, M., Lauvset, S. K., Grini, A., et al. (2018). Climate response to aerosol geoengineering: A multimethod comparison. *Journal of Climate*, *31*(16), 6319–6340. https://doi.org/10.1175/JCLI-D-17-0620.1

Myhre, G., Forster, P. M., Samset, B. H., Hodnebrog, Ø., Sillmann, J., Aalbergsjø, S. G., et al. (2017). PDRMIP: A precipitation driver and response model intercomparison project—Protocol and preliminary results. *Bulletin of the American Meteorological Society*, *98*(6), 1185–1198. https://doi.org/10.1175/BAMS-D-16-0019.1

Neale, R. B., & Hoskins, B. J. (2001). A standard test for AGCMs including their physical parameterizations:1:The proposal. *Atmospheric Science Letters*, *1*(2), 101–107. https://doi.org/10.1006/asle.2000.0019

Nie, J., & Sobel, A. H. (2015). Responses of tropical deep convection to the QBO: Cloud-resolving simulations. *Journal of the Atmospheric Sciences*, *72*(9), 3625–3638. https://doi.org/10.1175/JAS-D-15-0035.1

Niemeier, U., Schmidt, H., Alterskjaer, K., & Kristjánsson, J. E. (2013). Solar irradiance reduction via climate engineering: Impact of different techniques on the energy balance and the hydrological cycle. *Journal of Geophysical Research: Atmospheres*, *118*, 11,905–11,917. https://doi.org/10.1002/2013JD020445

Polvani, L. M., & Kushner, P. J. (2002). Tropospheric response to stratospheric perturbations in a relatively simple general circulation model. *Geophysical Research Letters*, *29*(7), 1114. https://doi.org/10.1029/2001GL014284

Rasch, P. J., Tilmes, S., Turco, R. P., Robock, A., Oman, L., Chen, C.-C., et al. (2008). An overview of geoengineering of climate using stratospheric sulphate aerosols. *Philosophical Transactions of the Royal Society A*, *366*, 4007–4037. https://doi.org/10.1098/rsta.2008.0131

Reichler, T., Dameris, M., & Sausen, R. (2004). Determining the lapse rate tropopause from gridded data. *Geophysical Research Letters*, *30*, 2042. https://doi.org/10.1029/2003GL018240

Richardson, T. B., Forster, P. M., Andrews, T., Boucher, O., Faluvegi, G., Flaschner, D., et al. (2018). Carbon dioxide physiological forcing dominates projected eastern Amazonian drying. *Geophysical Research Letters*, *45*, 2815–2825. https://doi.org/10.1002/2017GL076520

Richardson, T. B., Forster, P. M., Andrews, T., & Parker, D. J. (2016). Understanding the rapid precipitation response to CO_2 and aerosol forcing on a regional scale. *Journal of Climate*, *29*(2), 583–594. https://doi.org/10.1175/JCLI-D-15-0174.1

Richter, J. H., Tilmes, S., Glanville, A., Kravitz, B., MacMartin, D. G., Mills, M. J., et al. (2018). Stratospheric response in the first geoengineering simulation meeting multiple surface climate objectives. *Journal of Geophysical Research: Atmospheres*, *123*, 5762–5782. https://doi.org/10.1029/2018JD028285

Robock, A. (2000). Volcanic eruptions and climate. *Reviews of Geophysics*, *38*(2), 191–219. https://doi.org/10.1029/1998RG000054

Robock, A. (2008). 20 reasons why geoengineering may be a bad idea. *Bulletin of the American Meteorological Society*, *64*, 14–18.

Robock, A., MacMartin, D. G., Duren, R., & Christensen, M. W. (2013). Studying geoengineering with natural and anthropogenic analogs. *Climate Change*, *121*(3), 445–458. https://doi.org/10.1007/s10584-013-0777-5

Robock, A., Oman, L., & Stenchikov, G. L. (2008). Regional climate responses to geoengineering with tropical and Arctic SO_2 injections. *Journal of Geophysical Research*, *113*, D16101. https://doi.org/10.1029/2008JD010050

Samset, B. H., Myhre, G., Forster, P. M., Hodnebrog, Ø., Andrews, T., Faluvegi, G., et al. (2016). Fast and slow precipitation responses to individual climate forcers: A PDRMIP multimodel study. *Geophysical Research Letters*, *43*, 2782–2791. https://doi.org/10.1002/2016GL068064

Schmidt, H., Alterskjær, K., Karam, D. B., Boucher, O., Jones, A., Kristjánsson, J. E., et al. (2012). Solar irradiance reduction to counteract radiative forcing from a quadrupling of CO_2: Climate responses simulated by four earth system models. *Earth System Dynamics*, *3*(1), 63–78. https://doi.org/10.5194/esd-3-63-2012

Seager, R., Liu, H., Henderson, N., Simpson, I., Kelley, C., Shaw, T., et al. (2014). Causes of increasing aridification of the Mediterranean region in response to rising greenhouse gases. *Journal of Climate*, *27*(12), 4655–4676. https://doi.org/10.1175/JCLI-D-13-00446.1

Simpson, I. R., Blackburn, M., & Haigh, J. D. (2009). The role of eddies in driving the tropospheric response to stratospheric heating perturbations. *Journal of the Atmospheric Sciences*, *66*(5), 1347–1365. https://doi.org/10.1175/2008JAS2758.1

Simpson, I. R., Shaw, T. A., & Seager, R. (2014). A diagnosis of the seasonally and longitudinally varying midlatitude circulation response to global warming. *Journal of the Atmospheric Sciences*, *71*(7), 2489–2515. https://doi.org/10.1175/JAS-D-13-0325.1

Smyth, J. E., Russoto, R. D., & Storelvmo, T. (2017). Thermodynamic and dynamic responses of the hydrological cycle to solar dimming. *Atmospheric Chemistry and Physics*, *17*(10), 6439–6453. https://doi.org/10.5194/acp-17-6439-2017

Song, Y., & Robinson, W. A. (2004). Dynamical mechanisms for stratospheric influences on the troposphere. *Journal of the Atmospheric Sciences*, *61*(14), 1711–1725. https://doi.org/10.1175/1520-0469(2004)061<1711:DMFSIO>2.0.CO;2

Stenchikov, G. L., Kirchner, I., Robock, A., Graf, H.-F., Antunña, J. C., Grainger, R. G., et al. (1998). Radiative forcing from the 1991 mount Pinatubo volcanic eruption. *Journal of Geophysical Research*, *103*(D12), 13,837–13,857. https://doi.org/10.1029/98JD00693

Swain, D. L., Langenbrunner, B., Neelin, J. D., & Hall, A. (2018). Increasing precipitation volatility in twenty-first-century California. *Nature Climate Change*, *8*(5), 427–433. https://doi.org/10.1038/s41558-018-0140-y

Taylor, K. E., Stouffer, R. J., & Meehl, G. A. (2012). An overview of CMIP5 and the experiment design. *Bulletin of the American Meteorological Society*, *93*(4), 485–498. https://doi.org/10.1175/BAMS-D-11-00094.1

Tilmes, S., Fasullo, J., Lamarque, J.-F., Marsh, D. R., Mills, M., Alterskjaer, K., et al. (2013). The hydrological impact of geoengineering in the Geoengineering model Intercomparison project (GeoMIP). *Journal of Geophysical Research: Atmospheres*, *118*, 11,036–11,058. https://doi.org/10.1002/jgrd.50868

Tilmes, S., Richter, J. H., Kravitz, B., MacMartin, D. G., Mills, M. J., Simpson, I. R., et al. (2018). CESM1(WACCM) stratospheric aerosol geoengineering large ensemble project. *Bulletin of the American Meteorological Society*, *99*(11), 2361–2371. https://doi.org/10.1175/BAMS-D-17-0267.1

Tilmes, S., Sanderson, B. M., & O'Neill, B. C. (2016). Climate impacts of geoengineering in a delayed mitigation scenario. *Geophysical Research Letters*, *43*, 8222–8229. https://doi.org/10.1002/2016GL070122

Trenberth, K. E., & Dai, A. (2007). Effects of mount Pinatubo volcanic eruption on the hydrological cycle as an analog of geoengineering. *Geophysical Research Letters*, *34*, L15702. https://doi.org/10.1029/2007GL030524

Trisos, C. H., Amatulli, G., Gurevitch, J., Robock, A., Xia, L., & Zambri, B. (2018). Potentially dangerous consequences for biodiversity of solar geoengineering implementation and termination. *Nature Evology & Evolution*, *2*(3), 475–482. https://doi.org/10.1038/s41559-017-0431-0

Wittman, M. A. H., Charlton, A. J., & Polvani, L. M. (2007). The effect of lower stratospheric shear on baroclinic instability. *Journal of the Atmospheric Sciences*, *64*(2), 479–496. https://doi.org/10.1175/JAS3828.1

Xia, L., Nowack, P. J., Tilmes, S., & Robock, A. (2017). Impacts of stratospheric sulfate geoengineering on tropospheric ozone. *Atmospheric Chemistry and Physics*, *17*(19), 11,913–11,928. https://doi.org/10.5194/acp-17-11913-2017

Xie, S.-P., Deser, C., Vecchi, G. A., Ma, J., Teng, H., & Wittenberg, A. T. (2010). Global warming pattern formation: Sea surface temperature and rainfall. *Journal of Climate*, *23*(4), 966–986. https://doi.org/10.1175/2009JCLI3329.1

Yu, B., & Zwiers, F. W. (2010). Changes in equatorial atmospheric zonal circulations in recent decades. *Geophysical Research Letters*, *37*, L05701. https://doi.org/10.1029/2009GL042071